

# Attitude Control of a Tilt-rotor Tailsitter Micro Air Vehicle Using Incremental Control

Master of Science Thesis

G.H.L.H. Lovell-Prescod





# Attitude Control of a Tilt-rotor Tailsitter Micro Air Vehicle Using Incremental Control

Master of Science Thesis

by

G.H.L.H. Lovell-Prescod

to obtain the degree of Master of Science at the Delft University of Technology, to be defended publicly on  
Tuesday November 22, 2022.

Student number:	4371321	
Thesis committee:	Prof. Dr. G. C. H. E. de Croon	TU Delft, Chair
	Dr. Ir. E. J. J. Smeur	TU Delft, Supervisor
	Dr. C. Varriale MSc.	TU Delft, External
	Z. Ma MSc.	TU Delft, PhD Candidate

An electronic version of this thesis is available at <http://repository.tudelft.nl/>.



# Preface

This report serves to document the research carried out over the course of this thesis and is the culmination of the Master of Science degree in Aerospace Engineering. Within the wider context of micro air vehicle research, the research presented in this report aimed to solve issues regarding control and loss of control moment generation in tailsitters by means of thrust vectoring. The design and build of a tilt-rotor tailsitter micro air vehicle was presented along with the implementation of incremental nonlinear dynamic inversion for attitude control.

I would like to express my sincere gratitude to my daily supervisors Dr. ir. Ewoud Smeur and Ziqing Ma MSc. Their guidance and constructive feedback is reflected in the successes of this project. I would like to thank Dr. ir. Ewoud Smeur specifically for his understanding, flexibility and patience surrounding a profound personal loss of mine. Additionally, I would like to extend my appreciation to the MAVLab and its members (particularly Erik van der Horst) whose advice and help extended what this project was able to achieve.

*G.H.L.H. Lovell-Prescod  
Delft, November 2022*



# Table of Contents

<b>List of Tables</b>	<b>v</b>
<b>Introduction</b>	<b>1</b>
<b>I Literature Study</b>	<b>4</b>
<b>1 Hybrid MAVs</b>	<b>5</b>
1.1 Convertiplanes . . . . .	5
1.1.1 Tilt-rotor MAVs . . . . .	5
1.1.2 Dual-system MAVs . . . . .	7
1.1.3 Tilt-wing MAVs . . . . .	7
1.2 Tail-sitters . . . . .	7
1.2.1 Mono Thrust Transitioning . . . . .	8
1.2.2 Collective Thrust Transitioning . . . . .	8
1.2.3 Differential Thrust Transitioning . . . . .	9
<b>2 Control of Hybrid MAVs</b>	<b>10</b>
2.1 PID Control . . . . .	10
2.2 Optimal Control . . . . .	11
2.3 INDI Control . . . . .	13
2.3.1 Application of INDI Control in Literature . . . . .	15
<b>3 Combating Actuator Saturation</b>	<b>19</b>
3.1 Issues Related to Moment Generation . . . . .	19
3.2 Thrust Vectoring for Moment Generation . . . . .	21
<b>4 Research Gap</b>	<b>24</b>
<b>II Academic Paper</b>	<b>27</b>
<b>5 Conclusion</b>	<b>43</b>
<b>References</b>	<b>45</b>
<b>A Appendix</b>	<b>48</b>
A.1 Attitude Control . . . . .	48
A.2 Velocity Control . . . . .	49

# List of Symbols

## Abbreviations

AoA	Angle of Attack
CFD	Computational Fluid Dynamics
CG	Centre of Gravity
CTT	Collective Thrust Transitioning
DOF	Degrees of Freedom
DTT	Differential Thrust Transitioning
INDI	Incremental Nonlinear Dynamic Inversion
LQR	Linear-Quadratic Regulator
MAV	Micro Air Vehicle
MTT	Mono Thrust Transitioning
NDI	Nonlinear Dynamic Inversion
PID	Proportional-Integral-Derivative
PWM	Pulse Width Modulation
SISO	Single-Input Single-Output
UAV	Unmanned Aerial Vehicle
VTOL	Vertical Take-Off and Landing
WLS	Weighted Least Squares

## Roman Symbols

$\mathbf{F}_N^{\text{aero}}$	Vector of aerodynamic forces in the $Z_N$ -axis	[N]
$\mathbf{G}$	Control effectiveness matrix	[-]
$\mathbf{g}$	gravity vector	[m/s <sup>2</sup> ]
$\mathbf{I}$	Moments of interia matrix	[kg m <sup>2</sup> ]
$\mathbf{M}_{\text{tot}}$	Vector of total moments acting on body	[N m]
$\mathbf{M}_a$	Vector of moments due to aerodynamic effects	[N m]
$\mathbf{M}_c$	Vector of control moments	[N m]
$\mathbf{q}_{\text{err}}$	Quaternion attitude errors	[-]
$\mathbf{q}_{\text{ref}}$	Reference attitude in quaternion	[-]

$\mathbf{T}_N$	Thrust vector in the $Z_N$ -axis	[N]
$\mathbf{u}$	Vector of control inputs	[-]
$\mathbf{v}$	Vector of virtual commands	[rad/s <sup>2</sup> ]
$b$	Lateral distance from the c.o.g to the motors	[m]
$K_\eta$	Vector of attitude error gains	[-]
$K_\Omega$	Vector of attitude rate error gains	[-]
$L$	Moments about the $X_B$ -axis	[N m]
$l$	Longitudinal distance from the c.o.g to the hinge of each tilt mechanism	[m]
$M$	Moments about the $Y_B$ -axis	[N m]
$m$	mass	[kg]
$N$	Moments about the $Z_B$ -axis	[N m]
$p$	Roll rate	[rad/s]
$PP$	Propeller pitch	[m]
$q$	Pitch rate	[rad/s]
$r$	Yaw rate	[rad/s]
$T_0$	Static Thrust	[N]
$T_c$	Thrust corrected for inflow velocity	[N]
$T_l$	Thrust of the left motor	[N]
$T_r$	Thrust of the right motor	[N]
$T_Z$	Thrust is the $-Z_B$ direction	[-]
$v$	Airspeed/inflow velocity	[m/s]
$v_e$	Exit velocity	[m/s]
$X_B$	$x$ -axis in the body reference frame	[-]
$X_N$	$x$ -axis in the NED reference frame	[-]
$Y_B$	$x$ -axis in the body reference frame	[-]
$Y_N$	$x$ -axis in the NED reference frame	[-]
$Z_B$	$x$ -axis in the body reference frame	[-]
$Z_N$	$x$ -axis in the NED reference frame	[-]

### Greek Symbols

$\ddot{\xi}$	Vector of linear accelerations	[m/s <sup>2</sup> ]
$\delta$	Vector of tilt deflection angles	[rad]
$\dot{\Omega}$	Vector of angular accelerations	[rad/s <sup>2</sup> ]

$\Omega$	Vector of angular rates	[rad/s]
$\omega$	Vector angular velocities of the motors	[rad/s]
$\delta_l$	Deflection angle of left motor	[rad]
$\delta_r$	Deflection angle of right motor	[rad]
$\omega_c$	Corner frequency	[rad/s]
$\omega_l$	Angular velocity of the left motor	[rad/s]
$\omega_r$	Angular velocity of the right motor	[rad/s]
$\phi$	Roll angle	[rad]
$\psi$	Yaw angle	[rad]
$\tau_d$	time delay	[s]
$\theta$	Pitch angle	[rad]
$\zeta$	Damping ratio	[–]

# Introduction

Over the last few decades the use of unmanned aerial vehicles (UAVs) and more specifically micro air vehicles (MAVs) has seen tremendous growth. MAVs are increasingly being used for various applications spanning both the civilian and military spheres ranging from the inspection of infrastructure and the monitoring of crops to reconnaissance and surveillance missions. Such missions can demand the long range, high endurance, fast forward flight typical of fixed-wing MAVs whilst also requiring the utility of hovering and vertical take-off and landing which rotorcraft offer. Hybrid MAVs form a class of MAVs which feature a wing or wings for fast, efficient forward flight as well as the capabilities of vertical take-off and landing (VTOL) and hovering making them suitable for a very wide range of missions. It is this flexibility afforded in operation that has precipitated the increased interest in the design of this particular category of MAV over the last few years.

Hybrid MAVs can be divided into two broad categories namely: (1) convertiplanes and (2) tail-sitters, each of which can be further divided into a number of subcategories. Convertiplanes offer an approximately level platform throughout all phases of flight which is advantageous for the mounting of equipment. Different configurations of convertiplanes achieve this in different ways; one configuration, which is of particular interest to this research, is that of tilt-rotors. Tilt-rotors provide both vertical lift and horizontal thrust as well as control moments and forces (particularly in vertical flight) by tilting their rotors. Tail-sitters, which transition between flight phases by pitching up or down  $90^\circ$ , are an elegant physical solution to achieving vertical and horizontal flight. They are typically mechanically simple and inherently more efficient than convertiplanes because of the ability to use the same effectors for both phases of flight. With the increased operational flexibility afforded by hybrid MAVs comes a number of challenges which motivated this research and will be outlined in the following section.

## Motivation

What is true of all hybrid MAVs is that they are more difficult to control than either fixed-wing or rotorcraft MAVs because of the need to transition between vertical and horizontal flight phases as well as being more susceptible to gust disturbances. According to Smeur et al. [1] there are three major challenges when it comes to the development of hybrid MAVs, namely: (1) attitude control, (2) velocity control and (3) guidance, all three of which are related to the fact that hybrid MAVs operate in a large flight envelope including transition.

These issues are amplified in tail-sitter MAVs which trade mechanical simplicity for increased complexity involved in their control. Because tail-sitters transition by pitching up or down  $90^\circ$  they inevitably face very high angles of attack and therefore stalled flight. It is noted by Bronz [2], during the transition flight, flow separation caused by very large angles of attacks and a stalled wing can result in a loss of pitch moment generation for tail-sitters which rely on the diversion of propeller slipstreams for pitch moment generation. Additionally, during take-off, landing and vertical flight, tail-sitters struggle in the presence of wind, whether constant or in gusts. This is because of the orientation of tail-sitters during these phases of flight, i.e. pitched  $90^\circ$  upward with their wings perpendicular to any lateral wind. This can lead to actuator saturation during vertical flight and failed take-offs and landings reducing reliability.

Tail-sitters of the subcategory differential thrust transitioning (DTT) as described in [3] reduce the reliance on aerodynamic control surfaces alleviating issues related to flow separation and actuator saturation however do not make take-off and landing in windy conditions any

easier. It is proposed that by incorporating tilting rotors into the design of tail-sitters the aforementioned issues and challenges can be solved simultaneously and it is this hypothesis that has motivated the research presented in this report.

## Research logistics

The research presented in this report as well as the findings of the entire thesis project will be guided by the following research objective:

### Research Objective

To solve issues regarding control and loss of control moment generation by developing an INDI controller capable of controlling a novel configuration of tail-sitter MAV utilising thrust vectoring as its only means of actuation.

In order to achieve the above research objective the research question below is defined. Additionally this main research question can be split into multiple sub-questions which follow. The sub-questions will define the structure of the research and therefore also loosely define the structure of this report. The report structure will be outlined in the next section.

### Research Question

How can a tail-sitter MAV with a pair of tilttable propellers serving as its only effectors be controlled?

#### **Subquestions:**

1. What are the challenges currently faced when developing hybrid MAVs?
  - a) What is/are the problem(s) inherent with the physical design of tail-sitters and what mitigation strategies can be employed?
  - b) What is/are the problem(s) inherent with the physical design of tilt-rotors and what mitigation strategies can be employed?
  - c) What problems are faced as pertains the controllability of these types of MAVs?
2. What robust control strategies are employed for the control of hybrid MAVs?
  - a) What advantages do each flight control strategy provide?
  - b) Can (and if so how) the controller be implemented to control a tail-sitters and tilt-rotors?
3. Is the use of tilting propellers as means of moment generation beneficial?
  - a) How would one go about integrating thrust vectoring by means of two leading edge mounted tilttable props into a selected control law?
  - b) Does the use of tilt-props solve the issue of loss of moment generation during transition of tail-sitter MAVs, i.e. are they effective effectors?

## Definitions & Conventions

Throughout this report the following definitions and conventions will hold unless stated otherwise.

- Vertical flight is defined as flight where all lift is generated through propulsion and horizontal flight is defined as flight where lift is generated aerodynamically as a result of horizontal velocity.
- The body reference frame, denoted by the subscript  $B$  herein, is left-handed orthogonal with its origin centred at the aircraft's centre of gravity. It is defined such that the body  $x$ -axis ( $X_B$ ) lies within the aircraft's symmetry plane and typically points through the nose of the aircraft during horizontal flight, the body  $y$ -axis ( $Y_B$ ) points along the right wing and the body  $z$ -axis ( $Z_B$ ) completes the axis system.
- The North-East-Down reference frame, denoted by the subscript  $N$  herein, has its origin centred at the aircraft's centre of gravity. It is defined such that its  $x$ -axis ( $X_N$ ) points north parallel to the earth's surface,  $y$ -axis ( $Y_N$ ) points east parallel to earth's surface and its  $z$ -axis ( $Z_N$ ) pointing downwards towards the earth's centre.
- Roll ( $\phi$ ), pitch ( $\theta$ ) and yaw ( $\psi$ ) angles are defined as rotations around the  $X_B$ ,  $Y_B$  and  $Z_B$  axes respectively with their sign defined according to the right-hand rule.
- Moments about the  $X_B$  ( $L$ ),  $Y_B$  ( $M$ ) and  $Z_B$  ( $N$ ) axes are positive according to the right-hand rule.

## Report structure

This report is divided into two main parts. Part I presents the documentation of the Literature Study phase of the thesis and is structured as follows. A general overview of hybrid MAVs will be presented in Chapter 1 and will include the advantages and disadvantages of the various configurations of hybrid MAVs presented in literature. Chapter 2 introduces some of the key issues encountered in the control of hybrid MAVs and presents a number of robust control techniques from literature employed for the control of (tail-sitter) hybrid MAVs. This Chapter goes in depth into the application of INDI control for various configurations of tail-sitters and tilt-rotors. A parallel field of research involving the effectiveness of tilt-props versus traditional flaps for the generation of moments and whether tilt-props can sufficiently solve issues with actuator saturation will be discussed in Chapter 3. Lastly, synthesis of the findings of Chapters 1 to 3 in the form of uncovering a research gap which the remainder of this thesis aimed to fill will be presented in Chapter 4. Part II presents the Academic Paper. The academic paper documents the main findings of the thesis and is intended to also serve as a standalone document. The build and implementation of INDI control for a tilt-rotor tailsitter is presented along with the results of test flights involving transition between vertical and horizontal flight. Lastly, Chapter 5 presents the key findings of both the literature study as well as the academic paper.

Part I

Literature Study

# 1

## Hybrid MAVs

Hybrid MAVs, as briefly described in the introduction, feature a wing or wings for fast and efficient forward flight whilst also possessing VTOL and hovering capabilities. There are endless possible configurations that achieve this set of capabilities but most configurations of hybrid MAVs typically fall within two general categories, namely: 1) convertiplanes or 2) tail-sitters[3]. The key difference between these two categories has to do with how the overall orientation of the airframe changes when switching between the different phases of flight. The overall orientation of the airframe of a convertiplane remains the same through all phases of flight (i.e. they remain approximately horizontal through take-off/landing, horizontal flight and hovering) whereas tail-sitters transition between vertical and horizontal flight or transition into/out of a hover by pitching  $90^\circ$ .

In addition to the overarching advantages and disadvantages of hybrid aircraft, this defining difference between convertiplanes and tail-sitters presents advantages and disadvantages for either category which will be explored in this chapter. Even though this literature study is focused on the control of tail-sitter MAVs, it is useful to contrast the two categories of hybrid MAVs to garner a better understanding as to why one might opt for developing a tail-sitter versus a convertiplane. Additionally, a key element of this literature review is to explore the effectiveness of tilting motors, a defining characteristic of an entire subclass of convertiplane. First, the various subclasses of convertiplanes will be explored including examples in literature followed by those of tail-sitters.

### 1.1 Convertiplanes

The convertiplane category encompasses a wide range of configurations and can be further split into a number of subcategories including: dual-system, tilt-rotor and tilt-wing MAVs. Simple diagrams of generic configurations falling within the aforementioned subcategories are presented in Figure 1.1. In this section an brief description of the various subclasses of convertiplanes will be discussed along with their respective pros and cons. Common to all subcategories discussed below and therefore in addition to their respective pros and cons, one major advantage of convertiplanes is that they offer an approximately level platform for the mounting of equipment as they do not pitch  $90^\circ$  for transition. Usually, however, they have one or more effectors inoperable regardless of the phase of flight (e.g. flaps used during forward flight not being used during vertical flight etc.).

#### 1.1.1 Tilt-rotor MAVs

As the name suggests, tilt-rotor MAVs use the same set of rotors for lift during vertical flight and for thrust during horizontal flight by tilting their rotors. During vertical flight, the rotors

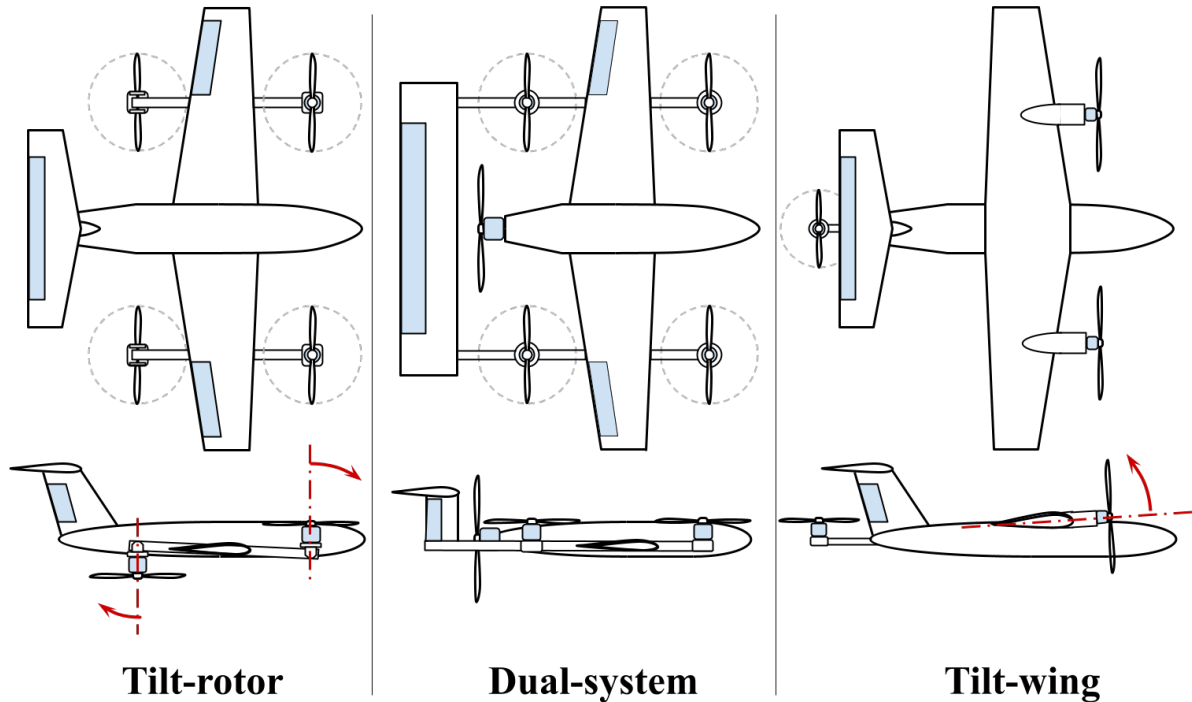


Figure 1.1: Generic examples of each subcategories of convertiplanes

(or a subset) are aligned such that the plane of rotation is horizontal and thus generating lift. Conversely, during horizontal flight the plane of rotation of the rotors is vertical providing horizontal thrust. During the transition from vertical to horizontal flight, as the plane of rotation tilts from horizontal to vertical the MAV gains horizontal speed and therefore gradually hands off lift generation from its rotors to its wing(s). A disadvantage of this configuration is the increased complexity of the system as a result of the tilting mechanism. This increased complexity inevitably adds weight and increases the likelihood of failures. However, as the rotors (or a subset of the rotors) have the dual function of providing both lift and thrust higher efficiency than Dual-system MAVs (discussed in Section 1.1.2) may be achievable. The configuration presented by Flores et al. [4] features four tilting rotors mounted to an otherwise conventional fixed-wing MAV. Wu et al [5] present a twin gimbaled tilt-rotor design similar to the Bell Boeing V-22 Osprey but with an additional propeller mounted to the tail. This tail mounted propeller provides additional thrust during horizontal flight improving transition and flight performance. Di Francesco et al. [6, 7] introduce a canard configuration with twin tilt-rotors mounted to the ends of the forewing. A third large, centrally mounted ducted fan provides most of the lift during vertical flight with the tilt-rotors mainly providing stability and control. Conventional control surfaces provide actuation during horizontal flight with the propulsive actuators (nacelle deflection and thrust setting of the tilt-rotors) stepping in in the event of actuator saturation. Raab et al. [8] present a hybrid MAV with two tilting rotors mounted at either end of the main wing and two fixed rotors fore and aft of the wing providing thrust in the negative  $Z_B$  direction exclusively. During hover and low flight speeds the four propellers provide lift with forward and backward accelerations provided with symmetric tilts of the tilt-rotors. Additionally, yawing moments in hover are generated with asymmetric tilting of the tilt-rotors, pitching moments generated with a differential change in thrust setting of the two fixed motors and rolling moments generated with differential thrust setting of the tilting rotors. During horizontal flight pitching moments are generated with an elevator and the fixed motors switched off. Another example of this configurations is presented in [9] which documents the physical and controller design of a tandem wing MAV with a central lifting fan beneath which

a vane is attached which can provide lateral thrust vectoring. Additionally this MAV has two thrust vectored engines mounted to the aft wing which provide stability in vertical flight and provide the thrust required in horizontal flight.

### 1.1.2 Dual-system MAVs

Dual-system MAVs have two independent propulsion systems. One system is entirely responsible for providing lift for vertical flight with the plane of rotation of the rotor(s) being horizontal whilst the other system is entirely responsible for the generation of thrust during horizontal flight (vertical orientation of the plane of rotation). A quad-plane, an example of this subclass of convertiplane, with 4 rotors responsible for vertical flight and a pusher propeller for thrust during wing-lifted flight is presented in [10]. The major advantage of this configuration is its simplicity; no additional mechanisms (which add complexity) are needed to orient the rotors depending on the phase of flight as independent systems are used for vertical and horizontal flight. Simplicity also extends to the controllability. Another advantage of this configuration is that the propeller pitch for either system can be optimised for efficiency for the specific flight modes in which they operate. A drawback to this configuration is that due to independent systems being used for the two flight modes, during one flight mode the systems required for the other are inactive and therefore simply a burden to the operative system (by either adding non-payload weight or by contributing to aerodynamic drag).

### 1.1.3 Tilt-wing MAVs

Similar to tilt-rotor MAVs, tilt-wing MAVs deliver VTOL and hovering capabilities along with fast, efficient horizontal flight by tilting the plane of rotation of the rotor, the difference being that instead of just the rotors being tilted, the plane of rotation of the rotors is tilted by tilting the entire wing to which the rotors are mounted. Examples of this configuration are outlined in [11] & [12], both featuring an auxiliary motor mounted at the tail for added stability during vertical flight. This subclass of convertiplane has the same advantages and disadvantages as tilt-rotor MAVs discussed above however they may have the added disadvantage of being more susceptible to disturbances due to cross-wind during vertical flight when the wing is in its vertical position. Additionally, tilt-wing MAVs have also to deal with high angles of attack resulting in flow separation over the wing and therefore control surfaces degrading their effectiveness. This does not affect a tilt-wings ability to transition as the transition of tilt-wing MAVs is not dependent on the control surfaces as is the case in many tail-sitters however as noted in [11] wing-fixed rolling moment generation (yawing moment generation from the body axes perspective) is very low in vertical flight. This is because of the effectivity of the control surfaces is dependent on the slipstream of the leading edge mounted propellers.

## 1.2 Tail-sitters

Tail-sitter MAVs take-off and land on their tails and transition between vertical and horizontal flight modes by pitching up or down  $90^\circ$ . The major advantage for the tail-sitter configuration being that the same set of effectors can be used during hovering, vertical and horizontal flight making the configuration inherently more efficient and less susceptible to failure; the less actuators required the less complex the mechanical design thus improving maintainability. On the other hand, as the same propulsion system provides both lift during vertical flight and thrust during horizontal flight the propeller pitch cannot be optimised for both conditions simultaneously requiring swashplates or variable pitch propellers should this optimisation be necessary. Furthermore, similar to tilt-wing MAVs characterised in Section 1.1.3, during vertical flight the wing is perpendicular to any crosswind potentially degrading performance whilst hovering. In [3], tail-sitters are classified into three categories, namely: mono thrust transitioning (MTT),

collective thrust transitioning (CTT) and differential thrust transitioning (DTT) MAVs (see Figure 1.2 for overview).

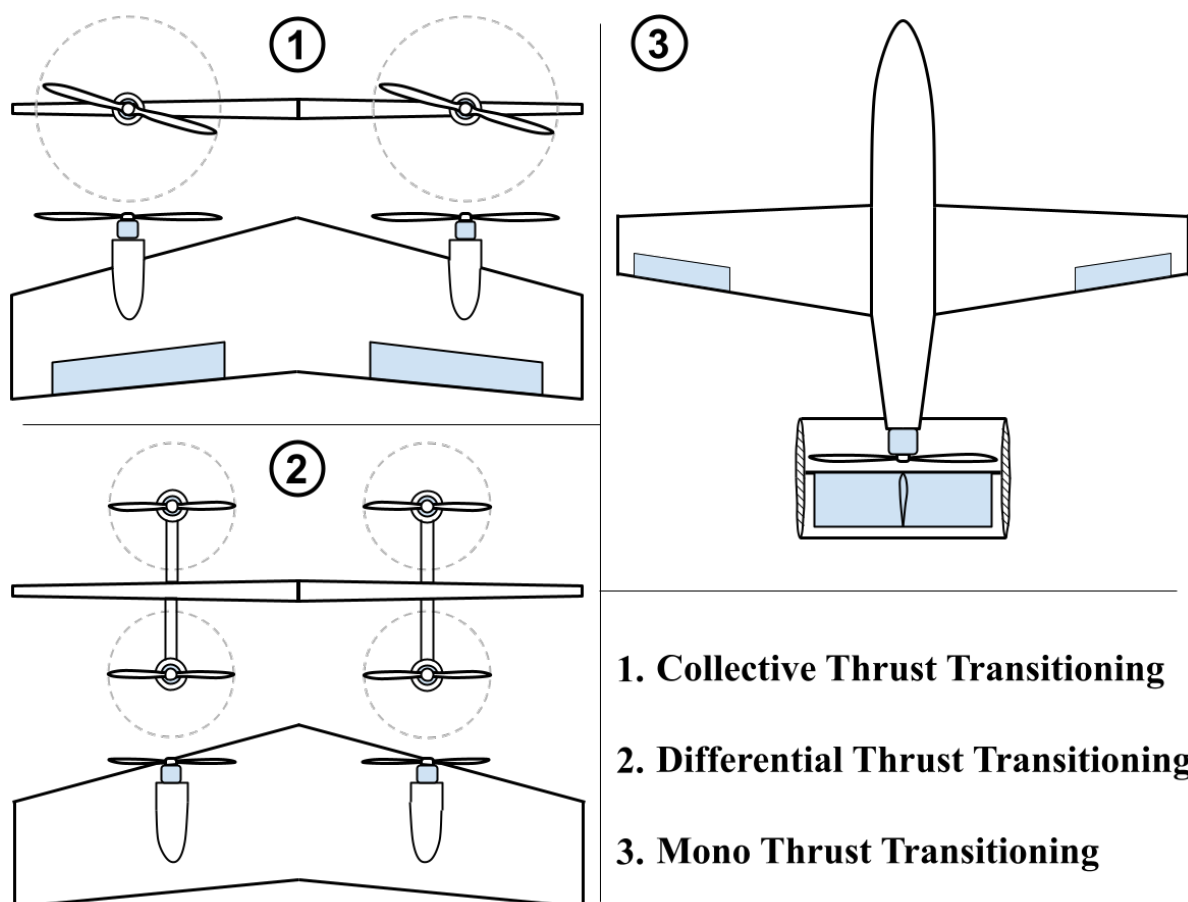


Figure 1.2: Generic examples of the subcategories of tail-sitters

### 1.2.1 Mono Thrust Transitioning

MTT tail-sitter MAVs utilise a single propulsion system for thrust generation. Typically this configuration involves a ducted fan with the moments required for transition being generated from thrust vectoring or ducted fan vanes. An example of this configuration is presented in [13] which features a large (relative to the overall size of the MAV) ducted fan to which wings are attached and behind which a cross tail with independent control surfaces is mounted. It makes use of stators designed such that they provide a rolling moment to counter the torque of the single ducted fan. Another such MTT tail-sitter is V-Bat outlined in [14] which features a single ducted fan mounted to the rear of an otherwise conventional configuration of MAV. Similarly, the tail-sitter used by Jung et al. in [15] for the development and application of a transition controller features a single rear mounted ducted fan attached to a large UAV stabilised with a canard forewing. It has vanes attached to the shrouding of the ducted fan to provide control moments during vertical and transition flight along with conventional aerodynamic control surfaces.

### 1.2.2 Collective Thrust Transitioning

CTT tail-sitter MAVs typically utilise fixed-pitch non-cyclical rotors and make use of control surfaces in combination with a collective variation in thrust[3]. The use of multiple rotors can provide increased control freedom compared to MTT tail-sitters however a potential problem faced by CTT tail-sitter MAVs is that during vertical flight control surfaces tend to be less

effective than during horizontal flight (or ineffective altogether) making control difficult with only two rotors. Tail-sitter MAVs of this class are presented in [1], [16], [17] and [18] all four of which feature a total of 4 effectors, two leading edge mounted propellers and two flaps which control 4 output degrees of freedom (DOF) namely: thrust, roll, pitch and yaw. The leading edge mounting of the motors provides effectiveness to the flaps during vertical flight due to prop-wash. The MAV presented in [19, 20] also falls within this category and features twin helicopter rotors mounted to each wing tip as well as flaps. This configuration is somewhat redundant as pitching and rolling moments can be generated not only by the flaps but also by cyclic variation of the helicopter rotors. Another tail-sitter falling into this category is the NederDrone [21], a hydrogen powered ‘drop-down’ tail-sitter with tandem wings mounted above and below its fuselage providing an offset in not only the horizontal direction but also in the vertical direction (from the level, forward flight perspective). The NederDrone features a total of 12 leading edge mounted motors (6 on each wing) and 8 flaps (4 on each wing) making it a highly redundant system from a control perspective. Differential thrust could conceivably be used to control roll, pitch and yaw control DOFs because of the configuration of the tandem wings although no specific mention of this was made in [21]. If this was the case this would also place this UAV in the category outlined next in Section 1.2.3.

### 1.2.3 Differential Thrust Transitioning

DTT tail-sitter MAVs use multiple rotors, typically symmetrically arranged about the fixed wing, to provide the actuation required for control. They utilise differential thrust to generate either (and in some cases all or any combination there of) pitch, roll and yaw moments in both horizontal and vertical flight. A major advantage of this configuration is that no involvement of control surfaces is required during vertical flight and strictly speaking the same is true of horizontal flight potentially limiting all moving parts to motors. One example of a DTT tail-sitter MAV is presented in [22] which is essentially a quadcopter embedded within a flying wing with the wing at a  $45^\circ$  angle to the cross formed by the arms of the 4 rotors. Another tail-sitter of this type is presented in [23] which features 4 rotors mounted to a flying wing airframe which provides full attitude and altitude control for both horizontal and vertical flight. The rolling moments (from the horizontal flight perspective, yawing moments in vertical flight) required to provide sufficient control authority in roll during level flight and wind disturbance rejection in vertical flight can exceed that of the rotor reaction torque. To combat this, the rotors are tilted slightly off axis such that there is a small component of thrust perpendicular to the axis between each rotor and the centre of gravity. This tilt of each rotor is arranged such that the moment created as a result is of the same sign as the rotors respective reaction torque. The Quadshot presented in [24] is another example of this type of tail-sitter.

# 2

## Control of Hybrid MAVs

Being capable of fast and efficient forward flight whilst simultaneously capable of VTOL and hovering, dictates that hybrid MAVs are inherently difficult to control. It is challenging to design controllers which perform adequately over the entire flight envelope. The varied flight envelope (from low-speed vertical flight to fast horizontal flight) means that controllers have to deal with significantly different dynamics presented by each flight phase [4]. During transition not only do hybrid MAVs experience highly nonlinear flight making modelling complex and expensive, they also encounter a change in the forces used to manipulate their accelerations. Furthermore, the ability to transition poses the challenge of how best to execute various flight manoeuvres, that is to say there is a choice as to whether to execute a manoeuvre entirely in one or other of the flight phases or whether to transition. Additionally, due to inevitable larger than normal (gust) disturbances during vertical/hovering flight due to the the large surface area of the fixed-wing which depending on the configuration can be perpendicular to the wind at times throughout the flight envelope. To effectively mitigate the inherent issues that accompany the benefits of hybrid MAVs, robust control techniques are necessary.

In this chapter the fundamentals of a number of control laws that have been implemented in literature for the control of hybrid MAVs will be outlined in detail. The following controllers will be outlined: PID control (Section 2.1), Optimal LQR control (Section 2.2) and Incremental Nonlinear Dynamic Inversion control (Section 2.3). The advantages and disadvantages of each controller will be discussed and in the case of PID and Optimal LQR control a brief overview of applications of these controllers in literature will be presented. A detailed review outlining the application of INDI control to various configurations of MAVs will be presented. This detailed review subsection was deemed necessary because of the focus of this literature study dictated by the research objective.

### 2.1 PID Control

A Proportional-Integral-Derivative (PID) controller provides continuous modulated control by providing a correction by means of proportional, integral and derivative terms to decrease a measured error  $e(t)$ , where  $e(t) = r(t) - y(t)$  and  $r(t)$  is a reference signal and  $y(t)$  is the process output. In its most basic form the controller output,  $u(t)$  is given by the following equation:

$$u(t) = K_P e(t) + K_I \int_0^t e(\tau) d\tau + K_D \frac{de(t)}{dt} \quad (2.1)$$

Where  $K_P$ ,  $K_I$  and  $K_D$  are the proportional, integral and derivative gains respectively. The proportional term, as the name suggests, provides a control output proportional to the error  $e(t)$ , i.e. if the error is positive and large the control output of this term is positive and large

taking into account the proportional gain  $K_P$ . The integral term provides a control output based on the cumulative error meaning that if a residual/steady-state error is present after the application of proportional control this integral term seeks to eliminate this residual/steady-state error. The derivative term utilises the current rate of change of the error to provide a control output and its main purpose is to suppress transient oscillations. A simplified block diagram of this type of controller is presented in Figure 2.1.

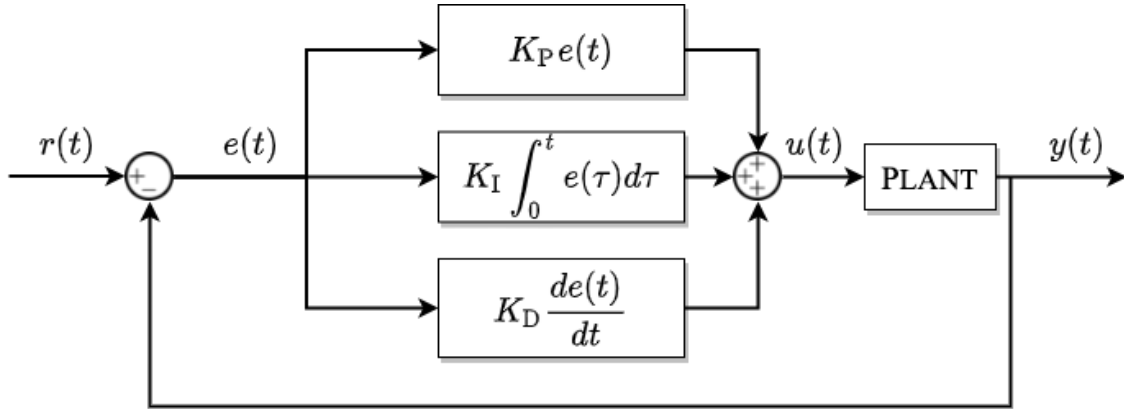


Figure 2.1: Block diagram of generic PID controller integrated into feedback loop

PID controllers can control the plant exploiting no knowledge of the system, by simply measuring the error  $e(t)$  and providing a linear control output to suppress this error. This can be seen as an advantage as complex (and therefore expensive) modelling, as would be the case for hybrid MAVs given the large flight envelope, is not required. The main limitation of PID controllers is that they are reactive controllers (counter errors which arise) meaning that often times the error must accumulate to trigger an adequate response from the integral term. This means they are not very robust against unknown disturbances to which gains cannot be preemptively tuned.

## PID Control in Literature

PID control has been applied to a wide variety of MAVs, including various configurations of hybrid MAVs. Additionally, applications range from being the sole controllers used to being used in conjunction with other controllers. PID control is the sole controller type implemented on the V-Bat (the details of which are presented in [14]) and is used for attitude control (quaternion based PID attitude controller) as well as guidance and velocity control. PID control is implemented on the Eye-On<sup>TM</sup> [4, 20] as the sole controller type for vertical flight (as one of two viable control laws used, the other being LQR control, see Section 2.2). PID control has also been implemented alongside other controllers like was done in [25] where a PID controller formed the outer loop guidance controller with an INDI attitude controller being the inner loop; this implementation was not the main focus of [25] but rather a controller design serving as a reference to which a cascaded INDI controller design was compared. Oosendo et al. in [22] make use of resolved tilt-twist feedback control method based on previous work [26] for the attitude control of a DTT tail-sitter MAV. The attitude error vector is the input to a PID controller whose gains are determined through the ultimate sensitivity method (Ziegler–Nichols tuning method) and tuned by trial and error.

## 2.2 Optimal Control

Optimal control is a branch of mathematical optimisation and a family of control techniques which seeks to control a system at minimum cost, i.e. optimal control seeks to obtain a control

law which minimises a cost function or simply put seeks to obtain an optimal control policy. One such optimal controller is the linear-quadratic regulator (LQR) which is likely one of the most important results in optimal control and is implemented for the control of a number of MAVs in one capacity or another.

The formulation of the LQR problem as outlined in [27] starts with considering a linear time-invariant state-space system of the following form

$$\dot{\mathbf{x}} = \mathbf{A}\mathbf{x} + \mathbf{B}\mathbf{u}, \quad \mathbf{x}(t_0) = \mathbf{x}_0 \quad (2.2)$$

Where  $\mathbf{x} \in \mathbb{R}^n$  is the state vector and  $\mathbf{u} \in \mathbb{R}^m$  the control command vector,  $\mathbf{A} \in \mathbb{R}^{n \times n}$  and  $\mathbf{B} \in \mathbb{R}^{n \times m}$  and for the infinite-horizon case which will be derived herein the conditions that the pair  $(\mathbf{A}, \mathbf{B})$  is controllable and  $\mathbf{x}_0$  is a (arbitrary) fixed initial state are set. The strategy, in its simplest form, computes a linear control law of the form,

$$\mathbf{u} = -\mathbf{K}\mathbf{x} \quad (2.3)$$

Where  $\mathbf{K} \in \mathbb{R}^{m \times n}$ , which minimises a quadratic cost function, e.g. the one given below in Equation 2.4

$$J = \int_0^{\infty} (\mathbf{x}^{\top} \mathbf{R} \mathbf{x} + \mathbf{u}^{\top} \mathbf{S} \mathbf{u}) dt \quad (2.4)$$

Where  $\mathbf{R} \in \mathbb{R}^{n \times n} = \mathbf{R}^{\top} \geq 0$  and  $\mathbf{S} \in \mathbb{R}^{m \times m} = \mathbf{S}^{\top} > 0$  making the cost function  $J \geq 0$  for the infinite-horizon case. The (optimal) LQR selected gain  $\mathbf{K}^*$  is given by,

$$\mathbf{K}^* = -\mathbf{S}^{-1} \mathbf{B}^{\top} \mathbf{Q} \quad (2.5)$$

Where  $\mathbf{Q} > 0$  for a controllable system and is found by solving the algebraic Riccati equation given by Equation 2.6.

$$\mathbf{A}^{\top} \mathbf{Q} + \mathbf{Q} \mathbf{A} - \mathbf{Q} \mathbf{B} \mathbf{S}^{-1} \mathbf{B}^{\top} \mathbf{Q} + \mathbf{R} = 0 \quad (2.6)$$

The main advantage of LQR controllers is that the optimal system input signal,  $\mathbf{u}$  is obtainable from full state feedback. In practice, however, full state feedback can be difficult to attain; in the case of a hybrid MAV, where stalled flight is inevitable, accurate feedback of the angle of attack for example is near impossible to obtain during transition which involves low airspeeds. Additionally, as can be seen from the above formulation of the LQR problem, a mathematical approximation of the the system is required in the form of  $\mathbf{A}$  and  $\mathbf{B}$  matrices of the state-space equation (Equation 2.2). Logically, the more accurate this mathematical approximation, the better the performance of such a controller, however, accurate models are both time-consuming and/or expensive to acquire.

## LQR in Literature

Lustosa et al. [28] conduct a windtunnel campaign to obtain a high-fidelity model used in the application of the LQR control law. Similarly, Forshaw et al. in [20] implement the LQR control law for vertical flight on a tail-sitter MAV with good results using a model developed with the aid of computational fluid dynamics (CFD). They did so along with the implementation of PID control to compare the two and found that the LQR controller was more robust to deviations in the equations of motion than the PID controller. Zhong et al. in [17] implement an LQR controller as the baseline controller for their tail-sitter MAV. This baseline LQR controller is augmented with an L1 adaptive controller to compensate for uncertainties arising in the dynamic equations of motion, namely uncertainties in best estimate of the inverse of the moments of inertia and the mathematical formulation of the aerodynamic moments.

## 2.3 INDI Control

Incremental nonlinear dynamic inversion (INDI) control is a sensor-based control technique resting on the notion that the sum of all forces/moments, both internal and external cause the linear/angular accelerations that can be measured (Newton's second law). This can be exploited to suppress unmodelled dynamics and disturbances making INDI capable of robustly controlling nonlinear systems subject to disturbances without an accurate (and therefore expensive) mathematical model. It does this by computing the required increment in control input to achieve the desired linear and angular acceleration at each sample time [16]. To compute these required increments in control inputs the only required knowledge is the control effectiveness (i.e. the change in force or moment resulting from a change in control input) and actuator dynamics should actuator feedback not be available.

INDI control is a variation of nonlinear dynamic inversion (NDI) control which involves the inversion of the plant dynamics for the control of nonlinear, control-affine systems, i.e. a system in which the states appear to vary linearly w.r.t the control inputs but the states vary nonlinearly w.r.t. to the states themselves. To understand INDI a brief look will be taken at NDI first.

### Nonlinear Dynamic Inversion

Given a nonlinear, control-affine single-input single-output (SISO) system in controllable canonical form given in Equation 2.7 the control input  $u$  can be arrived at as follows [29, Chapter 6]. The SISO case will be explored for simplicity's sake.

$$x^{(n)} = \mathbf{b}(\mathbf{x}) + \mathbf{a}(\mathbf{x})u$$

$$\frac{d}{dt} \begin{bmatrix} x_1 \\ \vdots \\ x_{n-1} \\ x_n \end{bmatrix} = \begin{bmatrix} x_2 \\ \vdots \\ x_n \\ \mathbf{b}(\mathbf{x}) + \mathbf{a}(\mathbf{x})u \end{bmatrix} \quad (2.7)$$

Where  $x$  is the scalar output,  $u$  the control input,  $\mathbf{x} = [x \ \dot{x} \ \dots \ x^{(n-1)}]^\top$  the state vector. A control input  $u$  of the form given in Equation 2.8 cancels out the nonlinearities to obtain an simple input-output relationship assuming  $\mathbf{a}(\mathbf{x}) \neq 0$ .

$$u = \mathbf{a}(\mathbf{x})^{-1} (v - \mathbf{b}(\mathbf{x})) \quad (2.8)$$

Where  $v = x^{(n)}$  is a virtual control input. A block diagram of the control law given in Equation 2.8 is presented in Figure 2.2.

The system may not be in controllable canonical form but rather a nonlinear, control-affine system of the form given below in Equation 2.9 then the NDI control law can be arrived at through input-output linearisation. For simplicity's sake the case of a SISO system will be discussed but can be generalised for multiple-input multiple-output (MIMO) systems as done in [29, Chapter 6].

$$\begin{aligned} \dot{\mathbf{x}} &= \mathbf{f}(\mathbf{x}) + \mathbf{g}(\mathbf{x})u \\ y &= h(\mathbf{x}) \end{aligned} \quad (2.9)$$

The first order differentiation of the output equation  $y$  is given by Equation 2.10 having made use of Lie derivatives where  $L_{\mathbf{f}}h(\mathbf{x}) = \nabla h(\mathbf{x})\mathbf{f}(\mathbf{x})$  and  $\nabla h(\mathbf{x}) = \frac{\partial h(\mathbf{x})}{\partial \mathbf{x}}$  is the gradient of  $h(\mathbf{x})$ .

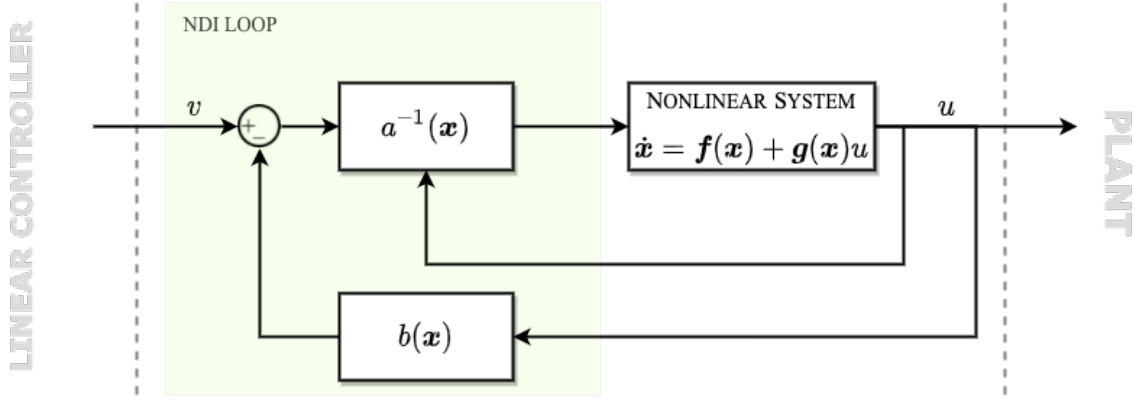


Figure 2.2: Block diagram of generic NDI control law

$$\begin{aligned}
 \dot{y} &= \nabla h(\mathbf{x}) \dot{\mathbf{x}} \\
 &= \nabla h(\mathbf{x}) \mathbf{f}(\mathbf{x}) + \nabla h(\mathbf{x}) \mathbf{g}(\mathbf{x}) u \\
 \Rightarrow \dot{y} &= L_{\mathbf{f}} h(\mathbf{x}) + L_{\mathbf{g}} h(\mathbf{x}) u
 \end{aligned} \tag{2.10}$$

If  $L_{\mathbf{g}} h(\mathbf{x}) = 0$  then Equation 2.10 can be iteratively differentiated until there exists a non-zero coefficient of the control input  $u$ . Equation 2.11 below characterises the  $r^{\text{th}}$ -order Lie derivative of the output  $y$  where  $r$  is the first positive integer of the series  $r = [1, 2, \dots]$  such that the coefficient of the control input  $u$  is a non-zero value. Note that the  $r^{\text{th}}$ -order Lie derivative of a function  $h(\mathbf{x})$  is given by  $L_{\mathbf{f}}^r h(\mathbf{x}) = L_{\mathbf{f}} [L_{\mathbf{f}}^{r-1} h(\mathbf{x})]$ .

$$y^{(r)} = L_{\mathbf{f}}^r h(\mathbf{x}) + L_{\mathbf{g}} L_{\mathbf{f}}^{r-1} h(\mathbf{x}) u \tag{2.11}$$

By introducing a virtual control input  $v = y^{(r)}$  the NDI control law can be obtained by rearranging Equation 2.11 as shown below where analogous expressions for  $\mathbf{a}(\mathbf{x})^{-1}$  and  $\mathbf{b}(\mathbf{x})$  from Equation 2.8 and Figure 2.2 become clear.

$$u = \frac{1}{\underbrace{L_{\mathbf{g}} L_{\mathbf{f}}^{r-1} h(\mathbf{x})}_{\mathbf{a}(\mathbf{x})^{-1}}} \left( v - \underbrace{L_{\mathbf{f}}^r h(\mathbf{x})}_{\mathbf{b}(\mathbf{x})} \right) \tag{2.12}$$

### Incremental Nonlinear Dynamic Inversion

The derivation of the the INDI control law aids in fundamental understanding and will therefore be derived in its most generalised form with guidance from [30]. Take, for example, a generalised nonlinear system given by Equation 2.13 where  $\mathbf{x}$  is the vector of states and  $\mathbf{u}$  the control command vector.

$$\dot{\mathbf{x}} = \mathbf{f}(\mathbf{x}, \mathbf{u}) \tag{2.13}$$

Note that unlike the derivation of the NDI control law, the INDI control law derivation begins from a more general system removing the constraint of being only applicable to control-affine systems. A first-order Taylor series expansion of this generalised nonlinear system approximates  $\dot{\mathbf{x}}$  for  $\mathbf{x}$  and  $\mathbf{u}$  in the region of  $(\mathbf{x}_0, \mathbf{u}_0)$  and is expressed as follows:

$$\dot{\mathbf{x}} \simeq \mathbf{f}(\mathbf{x}_0, \mathbf{u}_0) + \mathbf{F}_{\mathbf{x}} \Big|_{\substack{\mathbf{x}=\mathbf{x}_0 \\ \mathbf{u}=\mathbf{u}_0}} (\mathbf{x} - \mathbf{x}_0) + \mathbf{F}_{\mathbf{u}} \Big|_{\substack{\mathbf{x}=\mathbf{x}_0 \\ \mathbf{u}=\mathbf{u}_0}} (\mathbf{u} - \mathbf{u}_0) + \text{h.o.t.} \tag{2.14}$$

By definition the first term on the right hand side of Equation 2.14 is simply the state rate evaluated at  $\mathbf{x}_0$  and  $\mathbf{u}_0$  and can therefore be replaced by  $\dot{\mathbf{x}}_0$  ( $\dot{\mathbf{x}}_0 = \mathbf{f}(\mathbf{x}_0, \mathbf{u}_0)$ ). Additionally, for

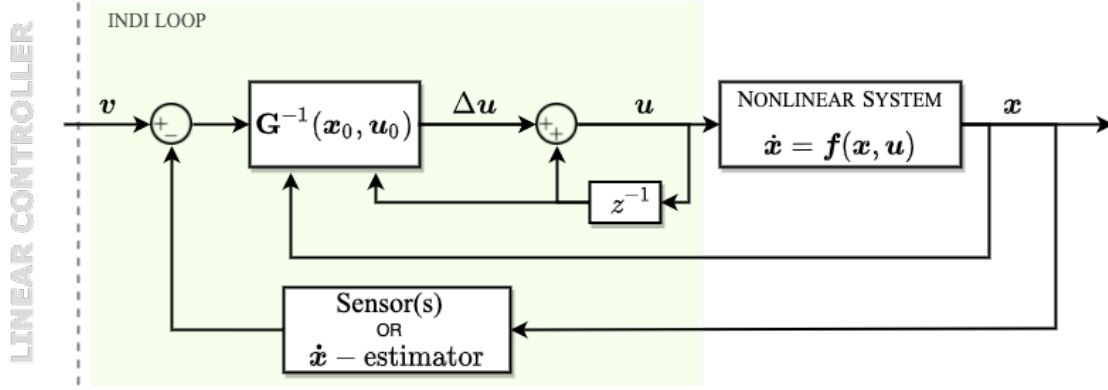


Figure 2.3: Block diagram of generic INDI control law

small time increments and assuming a sufficiently high control update rate it can be assumed that  $\mathbf{F}_x|_{\substack{x=x_0 \\ u=u_0}}(\mathbf{x} - \mathbf{x}_0) \ll \mathbf{F}_u|_{\substack{x=x_0 \\ u=u_0}}(\mathbf{u} - \mathbf{u}_0)$  and can therefore be neglected, giving rise to the following:

$$\dot{\mathbf{x}} \simeq \dot{\mathbf{x}}_0 + \mathbf{F}_u|_{\substack{x=x_0 \\ u=u_0}}(\mathbf{u} - \mathbf{u}_0) \quad (2.15)$$

Finally, inverting this simplified first order Taylor expanded expression, replacing  $\mathbf{F}_u|_{\substack{x=x_0 \\ u=u_0}}$  with  $\mathbf{G}(\mathbf{x}_0)$  for simplicity's sake and denoting the state rate,  $\dot{\mathbf{x}}$  as  $\mathbf{v}$  the generalised INDI control law is obtained and expressed in Equation 2.16 below.

$$\mathbf{u} = \mathbf{u}_0 + \mathbf{G}^{-1}(\mathbf{x}_0, \mathbf{u}_0)[\mathbf{v} - \dot{\mathbf{x}}_0] \quad (2.16)$$

Where  $\mathbf{v}$  is a vector of virtual commands,  $\dot{\mathbf{x}}_0$  are measured state rates and  $\mathbf{G}^{-1}(\mathbf{x}_0, \mathbf{u}_0)$  are control derivatives, also known as the control effectiveness matrix and is the only required knowledge in order to control this system. A block diagram of the control law given in Equation 2.16 is given in Figure 2.3.

The control effectiveness matrix  $\mathbf{G}^{-1}(\mathbf{x}_0, \mathbf{u}_0)$  is the only required knowledge in order to control this system which makes it an incredibly attractive control technique for hybrid MAVs which are inherently nonlinear systems and are particularly difficult to model because of needing to transition between vertical and horizontal flight phases.

### 2.3.1 Application of INDI Control in Literature

In this section a more detailed look at the application of the above theoretical formulation of the INDI control law to hybrid MAVs will be presented. INDI control for both attitude and velocity control will be discussed.

#### Attitude Control

INDI for attitude control rests on the notion that all moments acting on a rigid body, both internally and externally produce the angular accelerations of the said body. In literature, INDI for attitude control has been implemented for the control of a number of tail-sitters ([1], [16], [18]), tilt-rotors ([6], [8], [9]), a tilt-wing MAV ([11]) as well as for a quadcopter ([31]). The latter is relevant as its formulation can be generalised for an arbitrary configuration of MAV that uses thrust as the only means of actuation.

Yang et al. [16], Liu et al. [9] and Smeur et al. [31] all begin the formulation of the INDI control law for attitude control with the Euler's rotation equation which is given by

Equation 2.17. This equation expresses the total moments acting on a body in terms of the angular acceleration.

$$I\dot{\Omega} + \Omega \times I\Omega = M_{\text{tot}} \quad (2.17)$$

Where  $M_{\text{tot}}$  is further split into  $M_a$ , a the vector of moments as a result of aerodynamic effects of the airframe and  $M_c$ , a the vector of control moments. These control moments are generated through the deflection of aerodynamic surfaces and thrust. In [31], as the formulation is for a quadcopter, the reaction torques of the rotors  $M_r$  constitute a portion of  $M_{\text{tot}}$ . [16] and [31] continue by taking a first-order Taylor expansion of the above equation and making the assumption that partial derivatives w.r.t. states are far far smaller than w.r.t. control inputs arriving at the following expressions respectively.

$$\dot{\Omega} = \dot{\Omega}_0 + \left. \frac{\partial}{\partial \mathbf{u}} (I^{-1}M_c) \right|_{\substack{\Omega=\Omega_0 \\ \mathbf{u}=\mathbf{u}_0}} (\mathbf{u} - \mathbf{u}_0) \quad (2.18a)$$

$$\dot{\Omega} = \dot{\Omega}_0 + \left. \frac{\partial}{\partial \mathbf{u}} (I^{-1}(M_c - M_r)) \right|_{\substack{\Omega=\Omega_0 \\ \mathbf{u}=\mathbf{u}_0}} (\mathbf{u} - \mathbf{u}_0) \quad (2.18b)$$

Where the subscript ‘0’ indicates the current time or a time in the past. The current angular acceleration  $\dot{\Omega}_0$  encompasses all of the terms evaluated at the current rates and inputs. This  $M_c$  term ends up being the main contributor to the control effectiveness matrix for attitude control. Note that both [16] and [9] neglect  $M_r$  in their derivation. For simplicity’s sake the partial derivatives can be denoted by  $\mathbf{G}$ , known as the control effectiveness matrix and inverted to arrive at the INDI control law for attitude control (Equation 2.19). Note that this is of the same form as Equation 2.16.

$$\mathbf{u} = \mathbf{u}_0 + \mathbf{G}^{-1} (\mathbf{v} - \dot{\Omega}_0) \quad (2.19)$$

Where the control effectiveness matrix  $\mathbf{G}$  is comprised of an effectiveness value for each actuator on each controlled axis, i.e. comprised of effectiveness values  $G_{jk}$  which represent the effectiveness of actuator  $k$  on axis  $j$ . Additionally,  $\mathbf{v}$  a vector of virtual commands (the commanded angular acceleration).

The control effectiveness matrix  $\mathbf{G}$  contains the partial derivatives of  $M_c$  and  $M_r$  (and in principle even  $M_a$ ) w.r.t. the control inputs. It does not matter how this matrix is obtained. In Yang et al. [16] an expression for  $M_c$  specific to the THU-TS003 tail-sitter is given. This expression includes moment coefficients as functions the angle of attack  $\alpha$  and the sideslip angle  $\beta$ ; these moment coefficients were obtained through CFD modelling. Similarly Liu et al. [9] provides an expression for  $M_c$  also arrived at through CFD analysis. Smeur et al. [31] and Binz et al. [11] obtain this control effectiveness matrix through modelling  $M_c$  (as well as  $M_r$  in the case of the former) as a function of the control inputs analytically. Binz et al. [11] make use of a wing-fixed coordinate system to translate control moments generated by actuators fixed to the tilting wing to the body frame and this is reflected in the definition of  $M_c$ . Raab et al. [8] detail the control of a tilt-rotor MAV and calculate the control effectiveness matrices (or Jacobians as referred to in the paper) through the numerical differentiation of an ‘On Board Plant Model’. The approach adopted in Smeur et al. [1] is different in that it starts from Equation 2.19, i.e. is assumed that an increment in the inputs causes an increment in the angular acceleration according to the control effectiveness matrix  $\mathbf{G}$ . As that information must be contained in flight data,  $\mathbf{G}$  is build out in this way.

Interestingly, Yang et al. [16] note that in their case the control effectiveness matrix is mismatched with reality in the presence of gusts disturbances because the INDI is derived based on a nominal model. It was therefore decided to add an extra adjustable proportional

term to Equation 2.19 to strengthen the INDI controller in the presence of gust disturbances. This is dubbed Proportional-INDI or PINDI. The control input then becomes the following:

$$\mathbf{u} = \mathbf{u}_0 + \mathbf{G}^{-1} \left( \mathbf{v} - \dot{\boldsymbol{\Omega}}_0 \right) + \mathbf{K}_v \mathbf{I} \left( \dot{\boldsymbol{\Omega}} - \dot{\boldsymbol{\Omega}}_0 \right) \quad (2.20)$$

### Alternative Approaches

The approach to INDI attitude control outlined by Di Francesco et al. [6], though beginning with Euler's rotation equation like the sources outlined above, directly assumes that the control change  $\Delta \mathbf{u}$  that results in a desired change in angular acceleration  $\boldsymbol{\Omega}_d$  is given as follows.

$$\Delta \mathbf{u} = \left( \frac{\partial \mathbf{M}_c}{\partial \mathbf{u}} \right)^{-1} \left( \mathbf{I} \dot{\boldsymbol{\Omega}}_d - \mathbf{M}_{\text{tot}} + \boldsymbol{\Omega} \times \mathbf{I} \boldsymbol{\Omega} \right) \quad (2.21)$$

Di Francesco et al. [6] opt not to replace the last two terms of the above equation with measured or estimated angular accelerations because of concerns over time delays and noise. Instead an aerodynamic model of the aircraft is used.

Tal et al. [18] implement INDI control in a completely different way which does not involve linearisation of dynamics for inversion. Instead they makes use of a simplified  $\phi$ -theory aerodynamic forces and moments model to derive expressions for control inputs and states in terms of flat outputs allowing for fully nonlinear inversion (thus without requiring linearisation). Beginning with Euler's rotation equation given by Equation 2.17 above, the external moments  $\mathbf{M}_{\text{ext}}$  can be expressed as in Equation 2.22. Here 'external' means external to the modelled moments.

$$\mathbf{M}_{\text{ext}} = \mathbf{I} \dot{\boldsymbol{\Omega}}_0 - \mathbf{M}_0 + \boldsymbol{\Omega}_0 \times \mathbf{I} \boldsymbol{\Omega}_0 \quad (2.22)$$

Where, again, the subscript '0' indicates the current time or a time in the past.  $\mathbf{M}_0$  denotes the aerodynamic and thrust moments from calculated from the  $\phi$ -theory model with the current elevon deflections and motors speeds. Additionally,  $\dot{\boldsymbol{\Omega}}_0$  is obtained through the numerical differentiation of  $\boldsymbol{\Omega}_0$ . Equation 2.22 is then re-substituted into Euler's rotation equation. After making the assumption that the angular momentum cancels the measured angular momentum on the grounds that is slow changing and inverting the equation the following is obtained:

$$\mathbf{M}_c = \mathbf{I} \left( \dot{\boldsymbol{\Omega}}_c - \dot{\boldsymbol{\Omega}}_0 \right) + \mathbf{M}_0 \quad (2.23)$$

From the above equation the actuator commands can be calculated based on the defined model. Note that here the subscript 'c' represents 'commanded'.

### Velocity Control

Similarly to INDI for attitude control, INDI for velocity control rests on the notion that all forces acting on a body both internally and externally produce the linear accelerations that can simply be measured with accelerometers. A number of papers implement INDI velocity control. Smeur et al. [1] and Tal et al. [18] implement INDI velocity control for tail-sitters and Raab et al. [8] and Liu et al. [32] outline implementations for the velocity control of tilt-rotors. Newton's second law governs the translational dynamics and forms the basis of INDI velocity control in all aforementioned papers. In each paper Newton's second law takes on a form equivalent to Equation 2.24 below.

$$\ddot{\boldsymbol{\xi}} = \mathbf{g} + \frac{1}{m} (\mathbf{F}_N^{\text{aero}} + \mathbf{T}_N) \quad (2.24)$$

Where  $\ddot{\boldsymbol{\xi}}$  represents the second derivative of the position vector,  $\mathbf{g} = [0 \ 0 \ g]^\top$  is the gravity vector,  $m$  the mass of the MAV,  $\mathbf{F}_N^{\text{aero}}$  the aerodynamic forces in the NED frame (comprising  $\mathbf{L}_N$  and  $\mathbf{D}_N$ ) and  $\mathbf{T}_N$  the thrust vector also in the NED frame. Following the same steps as were

outline above all of these papers arrive at a INDI velocity control law resembling Equation 2.25 below except for [18] the details of which will follow.

$$\mathbf{v} = \mathbf{v}_0 + m\mathbf{G}^{-1} \left( \ddot{\boldsymbol{\xi}}_{\text{ref}} - \ddot{\boldsymbol{\xi}}_0 \right) \quad (2.25)$$

Where  $\mathbf{v}$  is the control vector and  $\mathbf{G}$  the control effectiveness matrix. This control effectiveness matrix encompasses the control derivatives pertaining both aerodynamic forces and thrust. In [25],  $\mathbf{v} = [\phi \ \theta \ T_{Z_B}]^T$  (tail-sitter and so thrust is only in the  $Z_B$ ). In [9],  $\mathbf{v} = [\alpha \ \beta \ \mu \ T_{X_B} \ T_{Y_B} \ T_{Z_B}]^T$ ; the MAV outlined in this paper is a tiltrotor with an additional vane mounted beneath a central lifting fan so thrust components are possible in all body axes.

### Alternative Approaches

The approach in Raab et al. [8] differs slightly as instead of explicitly using linear acceleration  $\ddot{\boldsymbol{\xi}}$  in their INDI control law, they use a vector of load factors  $\mathbf{n}$  in the control frame. The control effectiveness matrix is built out in the same way it was done for attitude control in this paper. That is, through the numerical differentiation of a plant model.

The approach outlined by Tal et al. [18] is analogous to the implementation of attitude control in the said paper. Through their flatness transform fully nonlinear inversion allows for the commanded attitude and commanded collective thrust to be calculated from the commanded force  $\mathbf{F}_c$ . Their flatness transform allows them to derive expressions for control inputs and states in terms of flat outputs. The commanded force is given in Equation 2.26 and is the INDI velocity control law.

$$\mathbf{F}_c = m(\ddot{\boldsymbol{\xi}} - \ddot{\boldsymbol{\xi}}_0) + \mathbf{F}_0 \quad (2.26)$$

Where the subscript ‘0’ indicates the current time or a time in the past.

# 3

## Combating Actuator Saturation

As discussed earlier, tail-sitter MAVs, though perhaps more complex from a control point of view, are mechanically simple in that, strictly speaking, the same actuators used for vertical flight can in many cases be used for horizontal flight as well. This, combined with the nature in which tail-sitters transition (i.e. by pitching up or down  $90^\circ$  and as a result inevitably experience stalled flight) means that the tail-sitter class of MAVs can be quite demanding of their actuators.

In this chapter the issue of actuator saturation or the inability to provide the required control moments will be explored. Examples of this issue coming up in literature will be presented followed by a possible solution.

### 3.1 Issues Related to Moment Generation

A common configuration of tail-sitter found in literature ([1], [16], [18], [17]) feature four actuators, namely two leading edge mounted motors and two flaps. An outline of the effect of these actuators on the control degrees of freedom is presented in Table 3.1. As defined in said table, the pitch angle  $\theta$  of the four outlined tail-sitters is controlled with a unidirectional change in the flap deflection  $\delta_{e_{l,r}}$  in both vertical and horizontal flight and the yaw angle  $\phi$  is controlled with a differential change in  $\delta_{e_{l,r}}$  in vertical flight. That is to say that both the pitching and yawing moments are generated exclusively or in part with the flaps making the flaps coupled effectors. According to Smeur et al. [1], the flaps are more effective during horizontal flight than during vertical flight. During vertical flight little to none of the airflow (in the leading edge to trailing edge direction) over the flaps is velocity induced airflow; little in the case of slow vertical climb and none in the case of hover. This means that most of the airflow which when deflected generate pitching and yawing moments is as a result of the slipstream of the leading edge mounted propellers (this is not the case for horizontal flight). In other words, during vertical flight pitching and yawing moment generation is dependent for the most part on the sections of the flaps which are ‘prop-washed’ meaning that attention must be placed either on the physical design of the propellers (to increase the proportion of the flaps which are prop-washed) or on the control allocation. Additionally as noted in [2] during the transition between vertical and horizontal flight, the issue of flow separation due to stall leads to the loss of pitching moment generation. This is reiterated in Smeur et al. [1], stating that on occasion, when flying at low airspeeds and high angles of attack the flaps saturate in an effort to provide enough pitching moment resulting in the Cyclone being “locked” in this state of not being able to pitch up sufficiently to transition from horizontal to vertical flight.

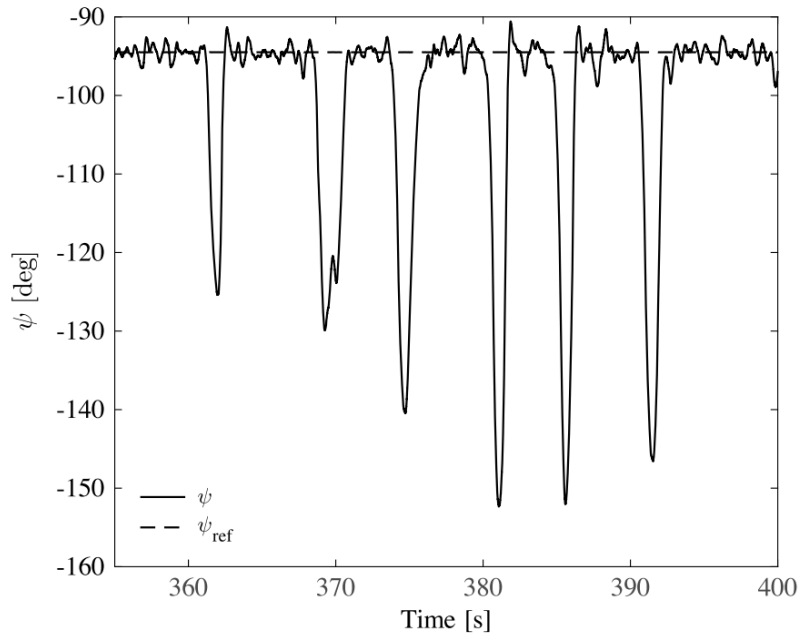
Actuator saturation is also an issue in the presence of large (constant) wind disturbances when significant if not all control effort is used up in trying to counter these disturbances meaning that little to no additional control authority can be allocated to guidance. Evidence of

Table 3.1: Table of the Actuators' effect on control DOFs

Control DOF	Vertical flight	Horizontal flight
Roll, $\phi$	Differential change in $\delta_{T_{l,r}}$	Differential change in $\delta_{e_{l,r}}$
Pitch, $\theta$	Unidirectional change in $\delta_{e_{l,r}}$	Unidirectional change in $\delta_{e_{l,r}}$
Yaw, $\psi$	Differential change in $\delta_{e_{l,r}}$	Differential change in $\delta_{T_{l,r}}$
Thrust, $T$	Unidirectional change in $\delta_{T_{l,r}}$	Unidirectional change in $\delta_{T_{l,r}}$

Where:  $\delta_e$  and  $\delta_T$  are the elevon deflection and thrust increment respectively

this is presented in Figure 3.1 where the Cyclone is commanded to track a reference yaw angle  $\psi_{\text{ref}}$  during hover in the presence of large lateral wind disturbances. A number of significant deviations from the reference yaw angle can be seen. Preceding each peak was the saturation of one of the flaps indicating that the maximum yaw control effort is reached on occasion.

Figure 3.1: Graph of yaw angle  $\psi$  of Cyclone showing unstable yaw manoeuvres [1]

In situations when the simultaneous control of both pitch  $\theta$  and yaw  $\psi$  (moments about the  $Y_B$  and  $Z_B$  axes) is required this issue of saturation is amplified as the already limited control effectiveness of the flaps must be shared between the two control DOFs.

Smeur et al. [1] deal with the Cyclone's shortcomings of this kind through control allocation and with specific design of the control effectiveness matrix. Control allocation typically refers to the challenge of distributing control effort over more actuators than controlled degrees of freedom but it also includes the distribution of control effort in the presence of actuator saturation. For the Cyclone, of the two control degrees of freedom controlled with the flaps, namely pitch  $\theta$  and yaw  $\psi$ , pitch was deemed the more important as the Cyclone was designed for passive stability during horizontal flight meaning pitching up  $90^\circ$  to return to hover is particularly difficult. As much control authority as is required or available should be allocated to pitch moment generation therefore. To this end, the weighted least squares (WLS) control allocation algorithm was employed as adapted to INDI control in [33] involving the construction and the minimising of a quadratic cost function involving relative weights for each controlled axis with a

higher relative weight being assigned to the pitch axis. Additionally, to give further impetus to the control authority over the pitch axis, control effectiveness of the motors on the pitch axis is sanctioned by adding a value to the corresponding elements of the control effectiveness matrix of the attitude controller ( $G_{jk}$  where ‘ $k$ ’ are the left and right motors respectively and ‘ $j$ ’ the pitch control degree of freedom).

Issues related to the saturation of the flaps are hinted at by Forshaw et al. in [19] which features the Eye-On<sup>TM</sup>, a tail-sitter MAV equipped with twin helicopter rotors along with flaps. During transition from vertical to horizontal flight the rotor system (which can provide pitching moments by means of cyclic variation) is used due to the inability of the flaps to provide sufficient pitching moments at low airspeeds; important to note in this case is that only a portion of the slipstreams of the rotors wash the flaps as the helicopter rotors are mounted to the wing tips. It is assumed that similar issues were experienced in the design of the THU-TS003 MAV presented in [16] as specific mention was made of the strong dependence on the slipstream of the propellers for attitude control along with two measures that were taken specifically to alleviate the control effort required to generate moments. Firstly, the propellers were designed such that most of the wing and flaps are in their slipstream. This has the side effect of reducing the local angle of attack prolonging the point at which stall and therefore flow separation leading to the loss of pitch moment generation occurs. Secondly, the flaps are large (approx. 30% of the wing surface area) and can deflect  $\pm 30^\circ$  giving substantial control authority to them. Zhong et al. in [17] also make mention of actuator saturation in tail-sitter MAVs and one of the main contributions of their paper is the presentation a control architecture that specifically takes into account input constraints on actuator deflections. It is postulated that during hovering the finite deflection of the control surfaces limit achievable performance and may even cause instability.

Further complicating all the issues advanced above is the fact that during vertical decent tail-sitters and other hybrid MAVs (like the design put forward in [11]) using prop-washed flaps/ailerons for pitch and/or yaw control can face flow reversal. That is to say, depending on the downward velocity of the vehicle the induced airflow in the trailing edge to leading edge direction may exceed the slipstream velocity of the propellers or at the very least will reduce the effectiveness of the prop-washed flaps. Additionally, it is conceivable that, depending on the proportion of the flaps that are prop-washed, the airflow reversal over the non-prop-washed portions of the flaps may result in a significant pitch moment generation in the opposite direction to the moments generated by the prop-washed portions reducing the overall effectiveness of the flaps.

## 3.2 Trust Vectoring for Moment Generation

The loss of moment generation due to flow separation experienced by hybrid MAVs like the Cyclone inspired the research presented in Bronz [2] which investigates through experimentation the effects of using thrust vectoring for control moment generation versus the use of traditional aerodynamic control surfaces. The experiment involves varying the deflection of leading edge mounted propellers over a series of angles between  $-30^\circ$  and  $+30^\circ$  and comparing the measured moment generated with that generated by the deflection of flaps over the same range of angles. Concrete conclusions can be drawn from this experiment as the motor-propeller combination is irrelevant during the comparison because the experiment is aiming to simulate the hovering flight phase, i.e. 0 m/s inflow velocity. This means that the only airflow which the flaps deflect to generate a moment is the slipstream of the same propeller-motor combination which is vectored by changing the angle of the propellers w.r.t. the wing. Should the experiment be conducted in the presence of external airflow a comparison could not be drawn. The experiment made use of a rectangular wing planform with a chord of 15cm and a span of 50cm with a flap of width equal to half the chord (0.5c) running the entire span of the wing.

The experiment found that the pitching moment generated by vectoring the thrust was almost two times that of the pitching moment generated by the same deflection of the flap for the same throttle setting and can be seen in Figure 3.2. The pitching moments generated by both the vectoring of thrust and the deflection of the flap both vary quasi-linearly for the range of angles used. Note that sign conventions are adopted such that a deflection of the same sign in both the flaps and the incidence of the propellers result in a moment of the same sign.

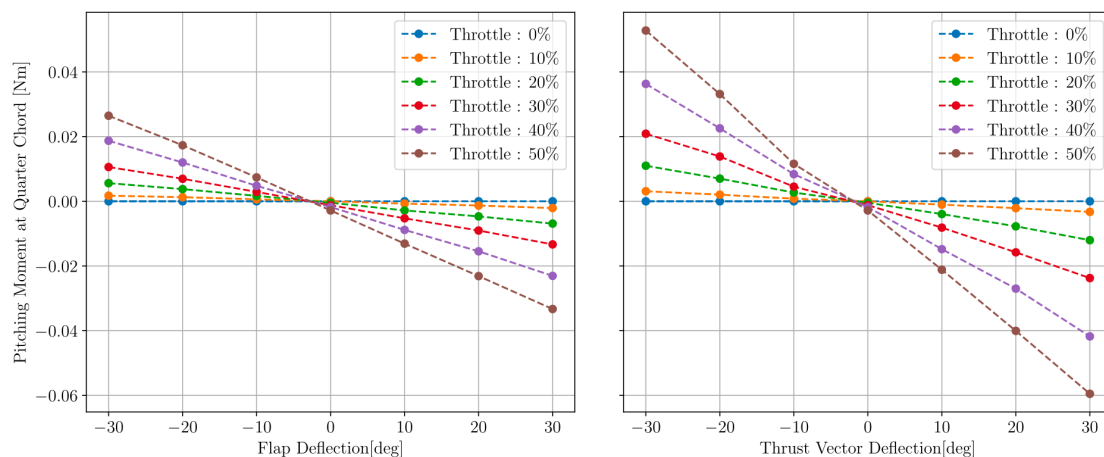


Figure 3.2: Comparison of pitching moment generated with flap deflection and thrust vectoring for a number of different throttle settings during experiments simulating hovering (0 m/s inflow velocity) [2].

In addition to thrust vectoring producing more pitching moment per degree is the fact that less lift is generated as a side effect of a change in commanded deflection. The deflection of a flap changes the camber and therefore the lifting properties of the wing; this is not the case with thrust vectoring and as a result less (unwanted) lift as a side effect is generated per degree of deflection comparatively. In situations where pure pitch is required this is quite attractive. The loss of this lifting force as a result of a deflection of the flaps may be seen as detrimental for yaw moment generation in vertical flight (moments about the  $Z_B$ -axis), however, so long as differential deflections of the propellers are possible this yaw control can still be achieved. Figure 3.3 shows lift as a side effect of the deflection of either the flap or the incidence angle of the propellers.

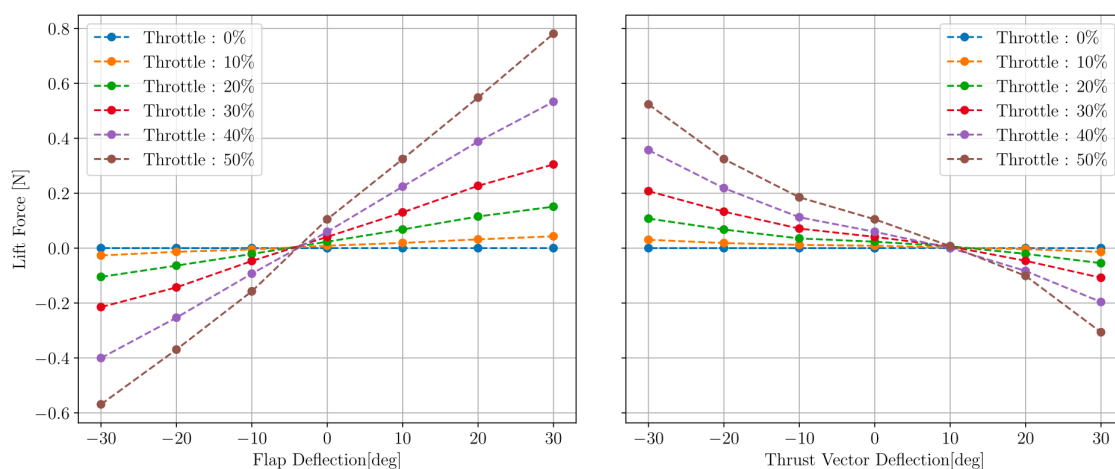


Figure 3.3: Comparison of lift generated with flap deflection and thrust vectoring for a number of different throttle settings [2]. Again, inflow velocity was 0 m/s.

This experiment demonstrates the viability of using thrust vectoring as a means of solving loss of control moment generation. Obviously, the idea of using thrust vectoring for the control of hybrid MAVs is not new, tilt-rotors are defined by their ability to use thrust vectoring as a means of control moment generation. Even though tilt-rotors do not transition between vertical and horizontal flight by pitching up or down  $90^\circ$  resulting in flow separation, their transition flight involves slow flight speeds leading to ineffective control surfaces. The tilt-rotor presented by Di Francesco et al. [6, 7] explicitly uses its tilt-rotors for control moment generation in the event of saturation of the aerodynamic surfaces during transition. Raab et al. [8] note that for slow flight speeds the elevator of their tilt-rotor is ineffective and therefore use thrust vectoring for control moment generation. This further demonstrates the viability of using thrust vectoring for solving loss of control moment generation of aerodynamic control surfaces.

# 4

## Research Gap

As alluded to in the research question outlined in the introduction a research gap lies where INDI control of a tail-sitter MAV and thrust vectoring as a means of control moment generation intersect. This research gap can be filled by investigating, designing (and building) and experimenting with the control of a tail-sitter MAV with a pair of tiltable propellers serving as its only effectors. The question then arises: “how would one go about integrating thrust vectoring by means of two leading edge mounted tiltable props into the INDI control law?”

A common configuration of tail-sitter found in literature features a flying wing or blended body airframe, 2 leading edge mounted motors and large prop-washed flaps. The Cyclone [1], the THU-TS003 [16] and the flying wing tail-sitter presented in [18] are all of this configuration. Assuming the experimental platform would take on a configuration somewhat similar, rolling moments during hover (moments about the  $X_B$ -axis) can be provided through differential thrust of the two motors and so there is little point in tilting rotors laterally as this would only add complexity for little to no extra control ability. Both pitch and yaw moment generation during hover i.e. moments about the  $Y_B$  and  $Z_B$  axes respectively (pitch and roll moment generation during level flight) can be provided by tilting the propellers in the same direction or differentially about an axis parallel to the  $Y_B$  axis respectively. In fact there exists in a flying wing with two tilting propellers serving as its only effectors presented by Garcia-Nieto et al. [34]. This hybrid MAV features two trailing edge mounted tilting propellers making it a ‘nose-sitter’. Garcia-Nieto et al. [34] focus on attitude tracking of their nose-sitter in hover by means of 4 linear PID controllers tuned by a genetic algorithm only partially exploring the main research gap of this thesis. INDI control of a tail-sitter actuated solely with two tilting motors has not been explored in literature to the best knowledge of the author. A possible implementation of INDI control for this type of tail-sitter will be explored briefly henceforth.

### INDI Velocity Control

In the case of a tail-sitter with two leading edge mounted tilting motors, the total thrust in the body frame  $\mathbf{T}_B$  becomes a function of the deflection angle of the left and right motors about their tilting axis. As motor deflections can be limited to deflections about an axis parallel to the  $Y_B$  axis only, the expression for thrust  $\mathbf{T}_N$  (from Equation 2.24) in the NED frame can be expressed as follows:

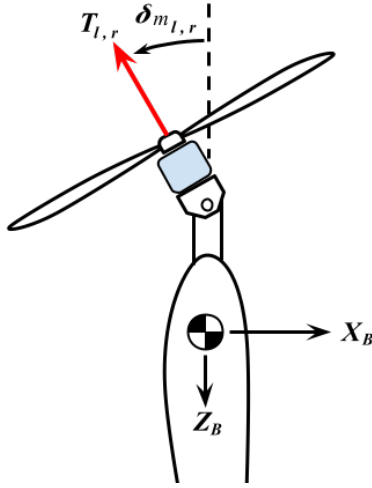
$$\mathbf{T}_N = \mathbf{M}_{NB} \begin{bmatrix} 0 \\ 0 \\ T_{Z_B} \end{bmatrix} = \begin{bmatrix} (s\theta c\psi + s\phi c\theta s\psi)T_{Z_B} \\ (s\theta s\psi - s\phi c\theta c\psi)T_{Z_B} \\ c\phi c\theta T_{Z_B} \end{bmatrix} \quad (4.1)$$

Where  $\mathbf{M}_{NB}$  is the transformation matrix from the body reference frame to the NED reference frame and is given by Equation 4.2 and  $T_{Z_B}$  is a function of the deflection angles of the left and

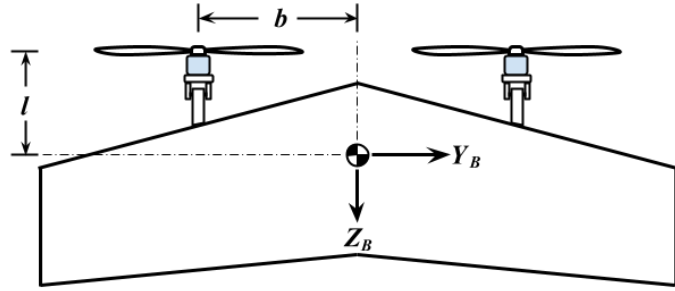
right motor(s) given by Equation 4.3.  $\delta_{m_l}$  and  $\delta_{m_r}$ , the deflection angles of the left and right motors respectively are defined according to Figure 4.1a.

$$\mathbf{M}_{NB} = \begin{bmatrix} c\theta c\psi - s\phi s\theta s\psi & -c\phi s\psi & s\theta c\psi + s\phi c\theta s\psi \\ c\theta s\psi + s\phi s\theta c\psi & c\phi c\psi & s\theta s\psi - s\phi c\theta c\psi \\ -c\phi s\theta & s\phi & c\phi c\theta \end{bmatrix} \quad (4.2)$$

$$T_{Z_B} = T_l \cos \delta_{m_l} + T_r \cos \delta_{m_r} \quad (4.3)$$



(a) Schematic showing definition of the deflection angle of the left & right motors  $\delta_{m_l}$  &  $\delta_{m_r}$ , respectively



(b) Schematic of top view showing definition of the motor positions w.r.t. the centre of gravity

Figure 4.1

The control effectiveness matrices can then be obtained using the method outlined in the ‘Velocity Control’ section of Section 2.3.1. A more complete derivation of velocity control utilising the above expressions can be found in Appendix A.

### INDI Attitude Control

INDI attitude control for the proposed experimental vehicle is relatively straightforward to formulate based on the method outlined in the ‘Attitude Control’ section of Section 2.3.1. Given that all the control moments of the proposed experimental vehicle are to be provided through thrust vectoring, the vector of control moments  $\mathbf{M}_c$  can be represented by simple dynamic equations. With the aid of Figure 4.1b which defines the motor location in the  $Y_B$ - $Z_B$  plane,  $\mathbf{M}_c$  is given by Equation 4.4.

$$\mathbf{M}_c = \begin{bmatrix} L \\ M \\ N \end{bmatrix} = \begin{bmatrix} -T_r b \cos \delta_{m_r} + T_l b \cos \delta_{m_l} \\ T_r l \sin \delta_{m_r} + T_l l \sin \delta_{m_l} \\ T_r b \sin \delta_{m_r} - T_l b \sin \delta_{m_l} \end{bmatrix} \quad (4.4)$$

Where  $T_l$  and  $T_r$  are the thrust of the left and right motors respectively and are functions of the angular velocity  $\omega$  of each motors. Additionally  $\delta_{m_l}$  and  $\delta_{m_r}$  are defined as in Figure 4.1a. A first order Taylor expansion of Euler’s rotation equation given by Equation 2.17 with the above expression for the vector of control moments leads one to an INDI attitude control law resembling Equation 2.19 with the control effectiveness matrix  $\mathbf{G}$  containing partial derivatives of  $\mathbf{M}_c$  w.r.t. the motor deflections of both left and right motors ( $\delta_l$  and  $\delta_r$  respectively) as well

as w.r.t. the angular velocities of both motors ( $\omega_r$  and  $\omega_l$ ). A more detailed derivation of the INDI attitude control law can also be found in Appendix A.

### Take-off and Landing Mechanics

As mention in the ‘Motivation’ section of the introduction, it is hypothesised that by incorporating tilting motors into the design of tail-sitters take-off and landing, performance can be improved. Tail-sitters are susceptible to being blown over during take-off because of the large surface area of the fixed wing. Similarly during landing, controllers may command pitch angles which deviate significantly from  $90^\circ$  (i.e. the vertical orientation) in an effort to combat lateral disturbances making landing challenging. It is proposed that the prototype should hinge  $90^\circ$  up about its trailing edge for take-off by tilting its motors accordingly, improving reliability. The opposite is proposed for landing, i.e. the prototype should hinge  $90^\circ$  down about its trailing edge. This would allow the tail-sitter to make contact with the ground at a wide range of pitch angles less than  $90^\circ$ . Figure 4.2 illustrates the take-off and landing mechanics of the proposed configuration which help improve reliability during take-off and landing.

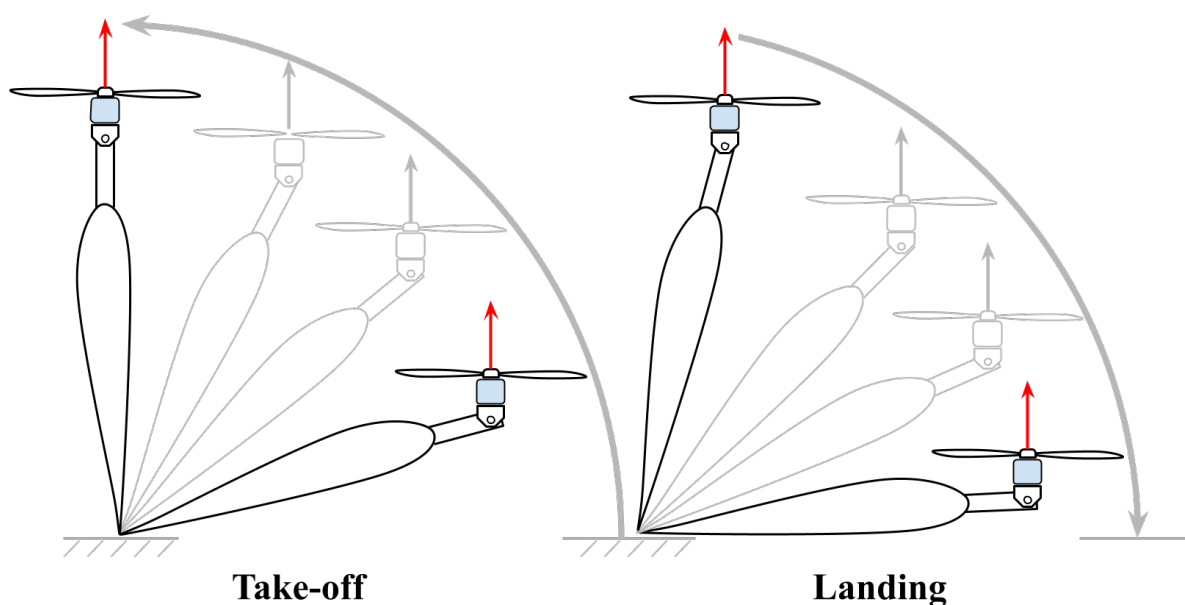


Figure 4.2: Diagram illustrating take-off and landing mechanics of the proposed configuration

**Part II**  
**Academic Paper**

# Attitude Control of a Tilt-rotor Tailsitter Micro Air Vehicle Using Incremental Control

G.H.L.H. Lovell-Prescod\*, Z. Ma†, E.J.J. Smeur‡, *Delft University of Technology, 2628 HS Delft, The Netherlands*

**Abstract**—By combining the ability to hover with a wing for fast and efficient horizontal flight, hybrid unmanned aircraft extend the flight envelope and therefore mission capabilities of unmanned aircraft. However, this comes at a cost: increased complexity control-wise and being more susceptible to wind disturbances. This susceptibility to wind gusts is particularly problematic for tailsitters as during hovering and vertical flight their wing is perpendicular to horizontal wind disturbances, often leading to actuator saturation. This paper presents a novel tailsitter micro air vehicle with two leading edge tilting rotors serving as its only actuators. It is shown that thrust vectoring generates sufficient control moment generation alleviating actuator saturation. Incremental nonlinear dynamic inversion (INDI) is implemented for attitude control and is demonstrated to compensate for unmodeled forces and moments whilst only relying on actuator control effectiveness and knowledge of actuator dynamics.

**Index Terms**—UAV, Tailsitter, Incremental control, INDI, Tilting rotors, Actuator saturation, Hybrid MAVs

## I. INTRODUCTION

OVER the last few decades the use of unmanned aerial vehicles (UAVs) and more specifically micro air vehicles (MAVs) has seen tremendous growth. MAVs are increasingly being used for various applications spanning both the civilian and military spheres ranging from the inspection of infrastructure and the monitoring of crops to reconnaissance and surveillance missions [1]. Such missions can demand the long range, high endurance, fast forward flight typical of fixed-wing MAVs whilst also requiring the utility of hovering and vertical take-off and landing which rotorcraft offer. Hybrids form a class of MAVs which feature a wing for fast, efficient forward flight as well as the capabilities of vertical take-off and landing (VTOL) making them suitable for a very wide range of missions.

These increased capabilities come at a cost. Hybrid MAVs, especially tailsitters, a subcategory of hybrid

MAVs which transition between horizontal and vertical flight by pitching either up or down  $90^\circ$ , are very difficult to control. The varied flight envelope comprising low-speed vertical flight, fast horizontal flight and the transition between the two means that the controller has to deal with significantly different dynamics presented by each flight phase[2]. This large, varied flight envelope makes mathematical modelling difficult and expensive. Even so, should a model be obtained, accurate state feedback required for such a model is difficult to measure over the entire flight envelope [3].

During transition tailsitters can experience a stalled wing due to high angles of attack. For tailsitters which use aerodynamic control surfaces the flow separation as a result of stall degrades control authority. Additionally, whilst in vertical flight tailsitters have their wing perpendicular to horizontal wind (gusts), requiring large control moments to counter [4]. To effectively mitigate these challenges careful consideration needs to be taken regarding (1) the selection and implementation of a control technique and (2) the effectiveness of actuators to provide the required forces and moments.

Lyu et al. [5] [6] implement PID attitude control on a quad rotor tailsitter with feedforward terms to cancel aerodynamic moments and the Coriolis term. Oosendo et al. [7] make use of resolved tilt-twist feedback control method based on previous work [8] for the attitude control of a tailsitter. The Attitude error was controlled using PID control which though simple is limited in disturbance rejection capabilities. Forshaw et al. [9] implement both PID control and linear-quadratic regulator (LQR) control on a tailsitter and found LQR control to be more robust to deviations in the equations of motion than PID control. The focus, however, of this paper was vertical flight and not the entire flight envelope. Lustosa et al. [10] implement a LQR controller for the optimal control of a tailsitter. Their approach, however, involved conducting a windtunnel campaign to obtain a high-fidelity model used in the application of the LQR control law; this is resource intensive and relies on full state feedback which in practice is difficult to reliably obtain during transition (high angles of attack and low

\* Graduate Student, MAVLab TU Delft, Kluyverweg 1

† Ph.D. Candidate, MAVLab TU Delft, Kluyverweg 1

‡ Assistant Professor, MAVLab TU Delft, Kluyverweg 1

airspeeds). Zhong et al. [11] cope with uncertainties arising in the mathematical formulation of the aerodynamic moments and estimate of moments of inertia by augmenting their LQR controller with an  $L_1$  adaptive controller.

One way to avoid resource intensive modelling is with the implementation of incremental nonlinear dynamic inversion (INDI) control. INDI control is a sensor-based control technique resting on the notion that the sum of all forces/moments, both internal and external cause the linear/angular accelerations that can be measured (Newton's second law). This can be exploited to suppress unmodelled dynamics and disturbances by computing the required increment in control input to achieve the desired linear/angular acceleration at each sample time. Smeur et al. [3] implement INDI control for both velocity and attitude control for the entire flight envelope demonstrating that all that is required for the robust control of a tailsitter is an expression for the effectiveness of the actuators on the control degrees of freedom. This expression for the effectiveness was acquired through test flights. Yang et al. [12] [13] and Tal et al. [14] also implement INDI control for the control of tailsitters. The former incorporate a mathematical model of the effectiveness of the actuators and the latter make use of a simplified  $\phi$ -theory aerodynamic forces and moments model to derive expressions for control inputs and states in terms of flat outputs allowing for fully nonlinear inversion. This allows the effective rejection of forces and moments external to the respective models. Raab et al. [15] and Binz et al. [16] implement INDI control for a tilt-rotor and a tilt-wing respectively with good results. The former obtaining an expression for the control effectiveness through the numerical differentiation of an onboard plant model and the later through mathematical modelling.

Additionally, the challenge of actuator saturation in tailsitters (especially around transition) is made mention of or alluded to in [11], [3] and [12]. During vertical flight, control moment generation almost entirely relies on the 'prop-washed' area of the flaps reducing their effectiveness. Furthermore, during transition, flow separation due to stall further degrades control effectiveness leading to potential saturation of the flaps. Bronz [4] proposes, therefore, that thrust vectoring be used as a means of control moment generation. It is shown through experimentation that the pitching moment generated through thrust vectoring was almost two times that of the pitching moment generated by the same deflection of the flap for the same throttle setting.

The contribution of this paper is the implementation of INDI control for a tilt-rotor tailsitter. The efficacy of control moment generation by means of thrust vectoring at

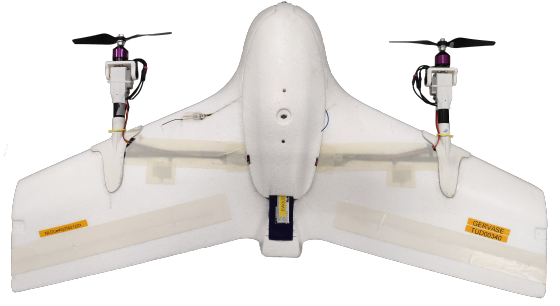


Fig. 1. Tiltprop tailsitter MAV used to conduct this research

combating actuator saturation is explored. Furthermore, it is demonstrated that the control derivatives for this configuration can be calculated analytically. This paper is structured as follows. First, the design of a tilt-rotor tailsitter MAV is outlined in section II. The rationale behind the conceptual design is also presented. The derivation and adaption of the INDI control law for said tilt-rotor tailsitter is presented in section III along with the actuator dynamics and other considerations necessary for the successful implementation. Test flight results are presented in section IV after which discussion and recommendations follow in section V. Finally conclusions are drawn in section VI.

## II. VEHICLE DESIGN

### A. Design conception

The design of the tilt-rotor tailsitter presented in this paper is influenced by the simplicity of a typical tailsitter as well as the challenges they face as a result. The tilt-rotor tailsitter shown in Figure 1 has four actuators to control four control degrees of freedom, namely: moments about the  $X_B$ ,  $Y_B$  &  $Z_B$  axes as well as the thrust in the  $Z_B$ -axis. The body axis system is defined as in Figure 2 and roll  $\phi$ , pitch  $\theta$  and yaw  $\psi$  refer to rotations about the  $X_B$ ,  $Y_B$  &  $Z_B$  axes respectively. The ZXY Euler rotation sequence is adopted throughout this paper to avoid singularities at  $\pm 90^\circ$  pitch [3].

Similar to tailsitters presented in [10], [11], [9], [3], [12], [14] this tilt-rotor tailsitter has two leading edge mounted motors. What sets it apart, however, is the fact that it has no aerodynamic control surfaces, instead it makes use of two servos which individually tilt the two motors. With this combination and number of actuators the four control degrees of freedom are controllable without any redundancy. Table I gives an overview of the effect of each actuator on the control DOFs.

As outlined in Table I and based on the body axis system defined in Figure 2 moments about the  $Y_B$ -axis and  $Z_B$ -axis are controlled with unidirectional and

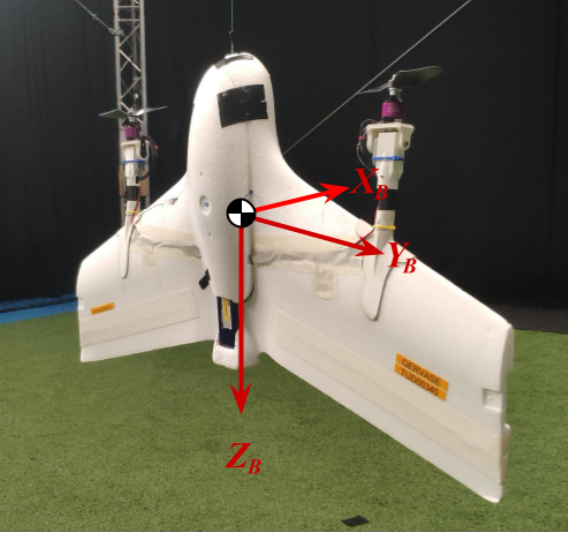


Fig. 2. Body axis system of the tilt-rotor tailsitter

TABLE I  
TABLE OF THE ACTUATORS' EFFECT ON CONTROL DOFS

Control DOF	Achieved with:
Moment about $X_B$ -axis, $L$	Differential change in $T_{l,r}$
Moment about $Y_B$ -axis, $M$	Unidirectional change in $\delta_{l,r}$
Moment about $Z_B$ -axis, $N$	Differential change in $\delta_{l,r}$
Thrust in $Z_B$ -axis dir., $T_Z$	Unidirectional change in $T_{l,r}$

Where:  $\delta_{l,r}$  and  $T_{l,r}$  are the left and right motor tilt angle and thrust respectively

differential changes in tilt angle  $\delta_{l,r}$  respectively. That is to say that the control effectiveness of the tilting of the motors is divided over two control DOFs. The servos actuating the tilt angle of the motors is analogous in purpose to the flaps in a typical tailsitter. A challenge common to said conventional tailsitters is actuator saturation. During horizontal flight sufficient airflow over the flaps results in adequate flap effectiveness. This is because during horizontal flight, in addition to the airflow due to propwash from the leading edge mounted motors, the velocity induced airflow over the flaps is significant. In vertical flight however, velocity induced airflow over the flaps is nonexistent in the case of hover, low in the case of slow vertical climb and negative in the case of descent. This degrades the flaps' control effectiveness. In the case of vertical descent the flow reversal over the flaps works against the already limited control effectiveness of the flaps further diminishing control authority. Additionally, during transition flow separation over the wing (and therefore flaps) leads to degraded control effectiveness making actuator saturation common [4]. The design of the tailsitter presented in this section aims at mitigating actuator saturation (experienced especially

TABLE II  
INVENTORY OF BUILD COMPONENTS

Component	Name	Qty.
Autopilot	mRo Pixracer R15	1
Motor	Hacker motors A20-20L EVO kV1022	2
ESC	T-motor F35A 3-6s	2
Servo	MKS HV9767	2
GPS	GPS NEO-M8N BDS Compass	1
Battery	Turnigy 3300mAh 4S 25C LiPo	1

around transition) not by overactuating the vehicle but rather by increasing the actuator control effectiveness by means of implementing thrust vectoring.

### B. Physical specifications

The airframe is the off-the-shelf Skywalker x5 EPO foam airframe into which two carbon fibre tubes were sunk allowing for the mounting of the left and right servos and motors. The airframe was stiffened laterally also using a carbon fibre tube. The tailsitter has a total mass of 1.27kg with a wingspan of 1.0m. The lateral distance of each motor from the centre of gravity is 0.3m (denoted herein by  $b$ ) with the longitudinal distance of the pivot of each tilting mechanism being 0.135m (denoted herein by  $l$ ); Figure 3 presents a schematic defining these distances. An inventory of the main electronic components used in the build is presented in Table II.

## III. ATTITUDE CONTROL

### A. Incremental Nonlinear Dynamic Inversion

INDI for attitude control rests on the notion that all moments acting on a rigid body, both internally and externally produce the angular accelerations of the said body which, conveniently, can be derived from gyroscope measurements. The derivation of the INDI control law for attitude control begins with Euler's rotation equation which is given by Equation 1 and expresses the total moments  $M_{tot}$  acting on a body in terms of the angular acceleration. This total moments can be expressed as the sum of two constituent components.

$$\begin{aligned} I\dot{\Omega} + \Omega \times I\Omega &= M_{tot} \\ I\dot{\Omega} + \Omega \times I\Omega &= M_c(\omega, \delta) + M_a(\Omega, v_B) \end{aligned} \quad (1)$$

Where  $M_a$  is the moment vector as a result of aerodynamic effects of the airframe and is therefore a function of the angular rates  $\Omega$  and the body velocity  $v_B$  and the control moment  $M_c$  is function of the angular rates of the motors  $\omega$  and the tilt angle of the left and right

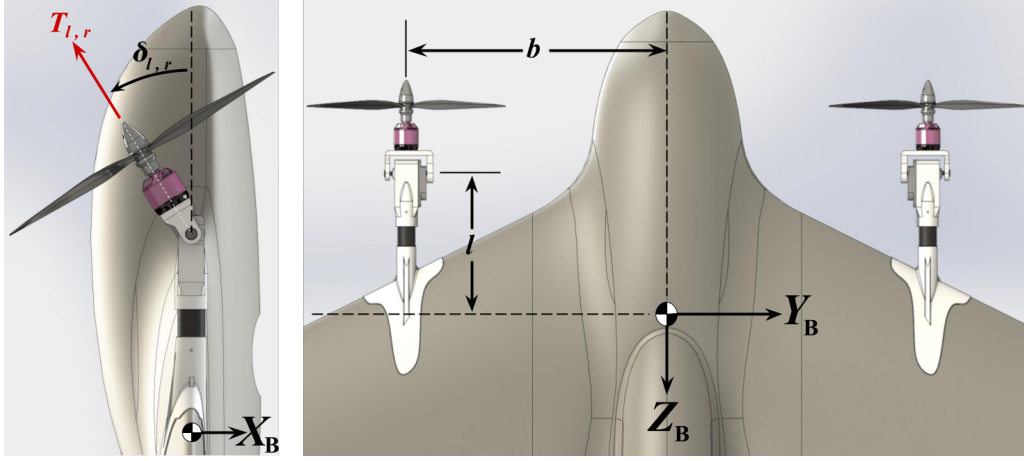


Fig. 3. Schematic showing definition of the deflection angle of the left & right motors  $\delta_l$  &  $\delta_r$  respectively as well as the scalar distances of each motor from the c.o.g.

motors  $\delta$  (both vectors) and is given by the following equation.

$$M_c = \begin{bmatrix} L \\ M \\ N \end{bmatrix} = \begin{bmatrix} -T_r b \cos \delta_r + T_l b \cos \delta_l \\ T_r l \sin \delta_r + T_l l \sin \delta_l \\ T_r b \sin \delta_r - T_l b \sin \delta_l \end{bmatrix} \quad (2)$$

Where  $T_l$  and  $T_r$  are the thrust of the left and right motors respectively and are functions of the angular velocity  $\omega$  of each motors. Additionally  $\delta_l$  and  $\delta_r$  are defined as in Figure 3.

Having rearranged Equation 1 into the expression below (Equation 3) one can take the first-order Taylor series expansion.

$$\dot{\Omega} = I^{-1} (M_a(\Omega, v_B) - \Omega \times I\Omega) + I^{-1} M_c(\omega, \delta_m) \quad (3)$$

Where the first term encompasses the moments independent of the actuators. The Taylor expansion then simplifies to the expression given in Equation 4 after grouping the terms evaluated at the current rates and inputs into the current angular acceleration  $\dot{\Omega}_0$ . It is assumed that the partial derivatives w.r.t. the  $\Omega$  and  $v_B$  have a far smaller effect than the partial derivatives w.r.t.  $\omega$  and  $\delta$ . This simplifying assumption is known as time scale separation and is valid when actuators are sufficiently fast and whose effect is much larger than aerodynamic moments due to changing angular rates and body speeds [17]. This assumption means that the remaining terms that need to be known for the implementation of INDI control only depend on the actuators. Dropping higher order terms and making a few simplifications, invert the resulting equality to arrive at the INDI control law.

$$\dot{\Omega} = \dot{\Omega}_0 + \left. \frac{\partial}{\partial \omega} (I^{-1} M_c(\omega, \delta_0)) \right|_{\omega=\omega_0} (\omega - \omega_0) + \left. \frac{\partial}{\partial \delta} (I^{-1} M_c(\omega_0, \delta)) \right|_{\delta=\delta_0} (\delta - \delta_0) \quad (4)$$

By substituting the expression for the vector of control moments given in Equation 2 the above equation can be expressed as follows in Equation 5.

$$\dot{\Omega} = \dot{\Omega}_0 + G(u - u_0) \quad (5)$$

Where the subscript '0' indicates the current time or a time in the past and the control input vector  $u$  is defined as follows:

$$u = [\delta_l \quad \delta_r \quad \omega_r \quad \omega_l]^\top \quad (6)$$

The control effectiveness matrix  $G$  is comprised of an effectiveness value for each actuator on each controlled axis, i.e. comprised of effectiveness values  $G_{jk}$  which represent the effectiveness of actuator  $k$  on axis  $j$ . At this point in the derivation it is useful to include the specific force in the negative  $Z_B$ -axis,  $T_Z$ . This is because the desired thrust in the  $Z_B$ -axis is fulfilled with the two motors which also have control authority over the other control DOFs meaning that the desired thrust increment must be allocated keeping into consideration the other control DOFs. Equation 5 becomes:

$$\begin{bmatrix} \dot{\Omega} \\ T_Z \end{bmatrix} = \begin{bmatrix} \dot{\Omega}_0 \\ T_{Z_0} \end{bmatrix} + G(u - u_0) \quad (7)$$

In the case of the tilt-rotor tailsitter presented in this paper the control effectiveness matrix  $G$  is defined analytically based on kinematics as in Equation 8.

$$\mathbf{q}_{\text{err}} = \mathbf{q}_{\text{ref}} \otimes \mathbf{q}_s^* \quad (12)$$

Where ‘ $\otimes$ ’ is the Kronecker product and the superscript ‘\*’ represents the conjugate. Both gains (i.e.  $K_\Omega$  and  $K_\eta$ ) can be tuned.

$$\mathbf{G} = \begin{bmatrix} \mathbf{I}_{\{3 \times 3\}}^{-1} & 0 \\ 0 & \frac{1}{m} \end{bmatrix} \cdot \begin{bmatrix} -bT_l s \delta_l & bT_r s \delta_r & -b \frac{\partial}{\partial \omega_r} (T_r) c \delta_r & b \frac{\partial}{\partial \omega_l} (T_l) c \delta_l \\ lT_l c \delta_l & lT_r c \delta_r & l \frac{\partial}{\partial \omega_r} (T_r) s \delta_r & l \frac{\partial}{\partial \omega_l} (T_l) s \delta_l \\ -bT_l c \delta_r & bT_r c \delta_r & b \frac{\partial}{\partial \omega_r} (T_r) s \delta_r & -b \frac{\partial}{\partial \omega_l} (T_l) s \delta_l \\ T_l s \delta_l & T_r s \delta_r & \frac{\partial}{\partial \omega_r} (T_r) c \delta_r & \frac{\partial}{\partial \omega_l} (T_l) c \delta_l \end{bmatrix} \quad (8)$$

Where ‘s’ and ‘c’ represent sine and cosine operations and  $b$  and  $l$  are the lateral distance of the thrust plane and longitudinal distances of the pivot of tilting motors respectively from the centre of gravity (see Figure 3) and  $m$  is the mass of the MAV. The order of the columns of the control effectiveness matrix  $\mathbf{G}$  are dictated by the definition of the control input vector  $\mathbf{u}$  (Equation 6). Equation 7 can simply be inverted to obtain the INDI control law and is given by Equation 9.

$$\mathbf{u}_c = \mathbf{u}_0 + \mathbf{G}^+ \left( \mathbf{v} - \begin{bmatrix} \dot{\boldsymbol{\Omega}}_0 \\ T_{Z_0} \end{bmatrix} \right) \quad (9)$$

Where the output of the equation  $\mathbf{u}_c$  is the new commanded inputs. The superscript ‘+’ represents the Moore-Penrose pseudoinverse,  $\mathbf{u}_0$  and  $\dot{\boldsymbol{\Omega}}_0$  the current control input vector and the measured angular acceleration vector respectively. Additionally,  $\mathbf{v}$  is a vector of virtual commands (the commanded angular acceleration). A summary of the control law in the form of a block diagram is presented in Figure 4.

The angular rates can be controlled with simple proportional feedback as shown in Equation 10 below.

$$\mathbf{v} = K_\Omega (\boldsymbol{\Omega}_{\text{ref}} - \boldsymbol{\Omega}) \quad (10)$$

The attitude can be controlled by a second proportional feedback controller using the feedback of the vector part of the quaternion error[18]:

$$\boldsymbol{\Omega}_{\text{ref}} = K_\eta \begin{bmatrix} q_{\text{err}1} \\ q_{\text{err}2} \\ q_{\text{err}3} \end{bmatrix} \quad (11)$$

Where the vector of quaternion errors  $\mathbf{q}_{\text{err}}$  represents the error between the reference attitude in quaternion form  $\mathbf{q}_{\text{ref}}$  and the state quaternion  $\mathbf{q}_s$  given by the following:

## B. Actuator Dynamics

In the above development of the INDI control law the need for knowledge of the plant dynamics is circumvented with the notion that these dynamics constitute the angular acceleration which are derived from measured gyroscope data. As a result the INDI control law relies heavily on the relationship between control inputs and measured outputs meaning knowledge of the actuator states is important. In the case of this tilt-rotor tailsitter where actuator state feedback is not readily available actuator dynamics are modeled. There are two types of actuators present in the MAV, namely: the tilting mechanism and the propulsion system. The dynamics of the tilting mechanism are driven mainly by the specifications of the MKS HV9767 servo and the moment of inertia of the tilts (motor mount, motor and propeller). The dynamics of the propulsion system are mainly dependent on the motor-propeller combination.

In order to identify the dynamics of the tilt mechanism an experiment was conducted following the experimental set up outlined in [19]. An MPU9255 Inertial Measurement Unit (IMU) was rigidly adhered to the tilt mechanism as shown in Figure 5 from which tilt angular rates are monitored and logged to SD card via an Arduino Due. Step changes in PWM commands were sent from the Arduino Due to servos for a number of different throttle setting also commanded by the Arduino Due.

Figure 6 shows the experimental data, i.e. the evolution of the angle of the servo as a response to a step input for different throttle settings. The tilt (servo plus motor, motor mount and propeller) dynamics were modelled as a second order system with delay and rate limit and this model is also shown in Figure 6. The second order transfer function of the tilt dynamics are characterised as follows:

$$A(s) = e^{-\tau_d s} \cdot \frac{\omega_c^2}{s^2 + 2\zeta\omega_c s + \omega_c^2} \quad (13)$$

Where  $\tau_d$  is the actuator delay,  $\omega_c$  is the actuator corner frequency and  $\zeta$  is the damping ratio. This response is then passed through a rate limiter with a rate limit corresponding to maximum observed angular rate during the experiments. The tilt dynamics are characterised in Table III. The equivalent discrete transfer function of

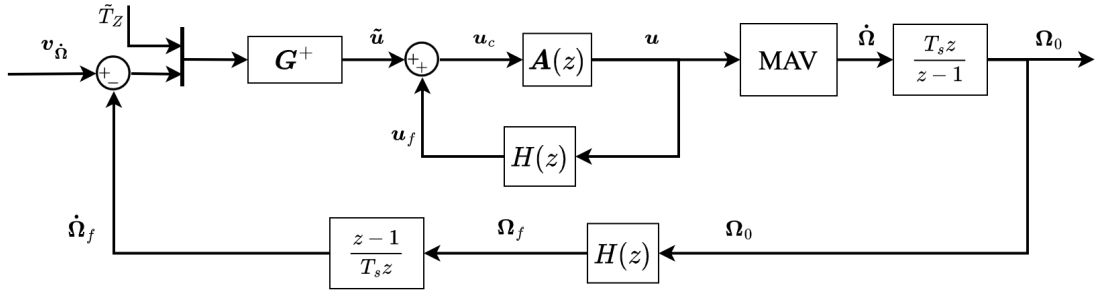


Fig. 4. Block diagram of the derived control law and its relation to the MAV

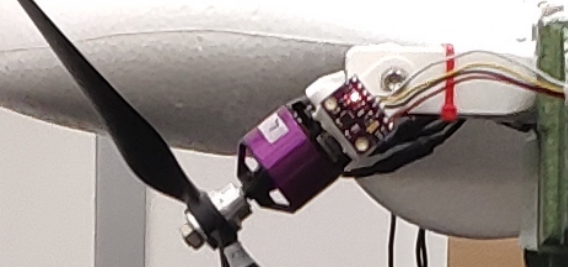


Fig. 5. Experimental setup of servo dynamics experiment

TABLE III  
SUMMARY OF ACTUATOR DYNAMICS CHARACTERISTICS

Tilt servo delay, $\tau_d$	14	[ms]
Tilt servo corner freq., $\omega_c$	76	[rad/s]
Tilt servo damping ratio, $\zeta$	0.8	[-]
Tilt servo rate limit	11.34	[rad/s]

the second order dynamics are given by the following equation for a sample frequency of 500 Hz the periodic frequency of:

$$A(z) = z^{-7} \cdot \frac{0.01175z^{-1} + 0.01079z^{-2}}{1 - 1.752z^{-1} + 0.7741z^{-2}} \quad (14)$$

### C. Implementation

The control law derived in subsection III-A was implemented along side the actuator dynamics modelled in subsection III-B within the Paparazzi open source autopilot software. A number of considerations have to be made for the successful implementation for the tilt-rotor tailsitter presented in this paper.

#### a) Filtering:

Firstly, the angular accelerations of the MAV are not measured directly but rather obtained through the differentiation of the measured angular rates from the onboard gyroscope. Inevitably, these measured rates will be noisy because of the presence of vibrations (e.g. induced by actuators) as well as noise simply inherent to the gyroscope. This noise is amplified after differentiation. The gyroscope measurements are passed, therefore, through a second-order Butterworth filter with a transfer function in the Laplace domain given by Equation 15. A corner frequency  $\omega_c$  of 6.28 rad/s (1 Hz) and damping ratio  $\zeta$  of 0.707. The equivalent discrete transfer function of said filter  $H(z)$  was used in the implementation and was obtained through the Tustin transform at 500 Hz.

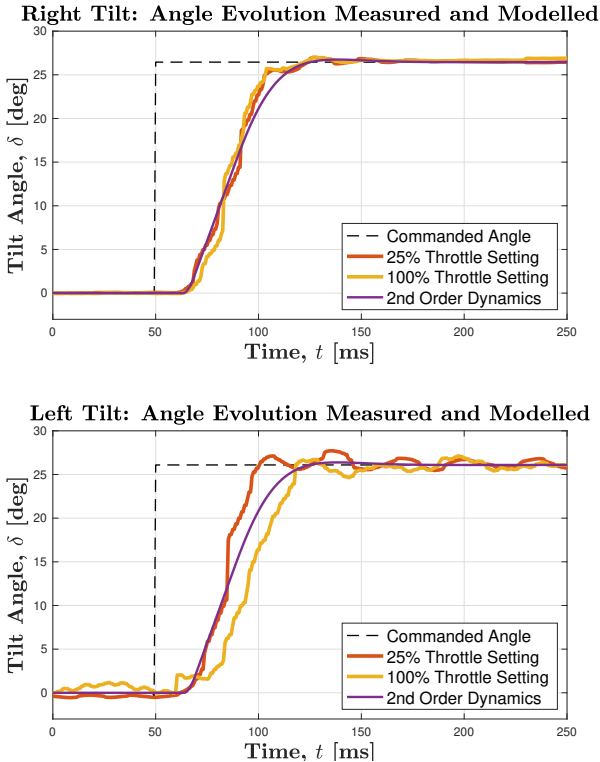


Fig. 6. Tilt angle response to a step input with throttle settings of 25% and 100% as well as 2<sup>nd</sup> order response to same step input.

$$\mathbf{H}(s) = \frac{\omega_c}{s^2 + 2\zeta\omega_c s + \omega_c^2} \quad (15)$$

The filtering of the angular rates introduces delay in the feedback and so to ensure synchronisation the actuator state feedback is also filtered with the same filter. Equation 9 can be updated as follows.

$$\mathbf{u}_c = \mathbf{u}_f + \mathbf{G}^+ \left( \mathbf{v} - \begin{bmatrix} \dot{\boldsymbol{\Omega}}_f \\ T_{Z_f} \end{bmatrix} \right) \quad (16)$$

Where the subscript ‘ $f$ ’ represents the filtered signal. Furthermore, as the axis about which the tilting mechanism rotates is parallel with the  $Y_B$ -axis additional noise is observed on the  $Y_B$ -axis of the gyroscope measurements. This noise propagates through the control loop via the calculation of the angular acceleration setpoint. A low-pass filter with corner frequency  $\omega_c$  of 12.56 rad/s (2 Hz) is introduced in the feedback of the body rates for the  $Y_B$ -axis. Equation 17 presents the transfer function of this filter; similarly, the equivalent discrete transfer function  $H_{LP}(z)$  was obtained with the Tustin transform at a sample frequency of 500 Hz

$$H_{LP}(s) = \frac{\omega_c}{s + \omega_c} \quad (17)$$

Equation 10 can be updated accordingly and is given by the following:

$$\mathbf{v} = K_{\Omega} \left( \boldsymbol{\Omega}_{\text{ref}} - \begin{bmatrix} p \\ q_{f_{LP}} \\ r \end{bmatrix} \right) \quad (18)$$

Where the subscript ‘ $f_{LP}$ ’ indicates the low-pass filtered signal.

Additionally, the tilt-rotors have a relatively large mass moment of inertia about the tilting axis (an axis parallel to the  $Y_B$ -axis) compared to that of the rest of the airframe. This relatively large moment of inertia coupled with the angular accelerations induced by the servos result in significant counter torques on the airframe. These counter torques initially cause an angular acceleration of the airframe in the opposite direction than desired which, in linear time invariant systems theory, is referred to as undershoot and is caused by nonminimum phase zeros [20, Ch. 8]. Based on angular accelerations of up to 176 rad/s<sup>2</sup> observed during the actuator tests, these counter torques can be as high as approximately 0.04 Nm and would otherwise make their way into the control loop via gyroscope measurements should lowpass-filtering not be implemented. The frequency content of these counter torques centre around the angular acceleration of the servos.

#### b) Control Allocation Priorities:

Calculating control inputs  $\mathbf{u}_c$  using the INDI control law given in Equation 16 does not guarantee that the control inputs satisfy Equation 19 below, i.e. the computed control inputs may exceed actuator limits.

$$\mathbf{u}_{\min} \leq \mathbf{u}_c \leq \mathbf{u}_{\max} \quad (19)$$

Simply clipping the computed control inputs such that the above condition is met leads to different control moments and forces than desired. It is therefore necessary to implement some sort of control allocation. Though control allocation typically refers to the challenge of distributing control effort over more actuators than controlled degrees of freedom it also includes the distribution of control effort in the presence of actuator saturation. To this end, the weighted least squares (WLS) control allocation algorithm was employed as adapted to INDI control in [21] in order to respect actuator limits as well as prioritisation.

In the case of this tilt-rotor tailsitter the four control DOFs are controlled with four actuators, two servos which manipulate tilt or deflection of the remaining two actuators, the two motors. A change in any one actuator’s command simultaneously affects the control effectiveness of that actuator on the moments about the  $X_B$ -,  $Y_B$ -,  $Z_B$ -axes and crucially the thrust in the negative  $Z_B$ -axis direction. A conceptual problem arises as a result pertaining to the prioritisation of control DOFs. Take for example a situation where the tilt-rotor tailsitter is in vertical flight in the presence of significant roll, pitch and yaw disturbances requiring sizeable deflections of the tilts as well as asymmetric thrust. The control allocation solution in this case may not satisfy all control objectives as unfeasibly large control objectives cannot be achieved with limited control authority. Conceptually it is more important that the MAV stays airborne rather than fulfills the other control moment objectives and as such priority should be given to the  $T_Z$  control DOF. In this implementation the relative priority factors fed to the WLS control allocation algorithm are [1, 1, 1, 10] for rotations around the  $X_B$ -,  $Y_B$ -,  $Z_B$ -axes and thrust in the negative  $Z_B$ -axis direction respectively. Depending on the scale of the control objectives this does not necessarily mean that the thrust in the negative  $Z_B$ -axis direction will take precedent over the others.

#### c) Imposing Lower Bound on Throttle:

Additionally if the throttle of one or both motors is ramped down to 0% the control effectiveness of the associated tilt becomes 0 creating an impossibility for the control allocation algorithm. This is because the control

DOFs and therefore associated control objectives can no longer be controlled. To prevent this, for vertical flight, a minimum throttle setting of 4000 on the range [0 9600] referred to herein as the Paparazzi scale is added, this is equivalent to 41.6% throttle setting per motor. For horizontal flight, a minimum of 2000 on the Paparazzi scale (21% per motor) is set. Note that nominal hover throttle setting is approximately 70% leaving sufficient room for differential thrust. Imposing this lower bound on the throttle setting of each motor has the bonus effect of also lower bounding the control effectiveness of the tilts on the respective control DOFs. This means that the commanded (and therefore required) increments are decreased.

*d) Constraining Control Objective:*

The development of the INDI control law in this section and the implementation of it making use of WLS control allocation relies on the linearisation of the actuator control effectiveness. It is important to bound the control objective to constrain the solution to the vicinity of the linearisation point. This can be done in two ways: by constraining the maximum increments of the actuators and/or by limiting the maximum angular rates used to calculate the control objective. A maximum increment of 4500 on the Paparazzi scale (equivalent to 25 deg) is set for each tilt. This value was chosen having compared the angular acceleration computed with the linearised control effectiveness (linearised about the zero tilt point, Equation 8) versus with the nonlinear equations for the control moments (Equation 2). It was found that a tilt increment of about 25 deg resulted in an error of 3.3%, an acceptable upper limit. Maximum roll, pitch and yaw rate setpoints of  $\pm 2$  rad/s (approx. 115 deg/s) were set. This also constrains the control law output to the vicinity of the point around which linearisation is conducted.

*e) Thrust equation & Servo Mapping:*

The final two components needed for the implementation of the control law derived in subsection III-A are an expression for the thrust as a function of the angular rate  $\omega_{l,r}$  and the linear mapping between the servo command and the tilt angle  $\delta_{l,r}$ . Static thrust tests using the RCBenchmark 1580 motor test bench logging thrust, electronic speed control (ESC) command and electronic RPM were conducted<sup>1</sup>. The following expression was obtained for the thrust in N for the motor-ESC pair outlined in subsection II-B.

$$T_{l,r}(\omega_{l,r}) = 5e - 6\omega_{l,r}^2 - 0.0008\omega_{l,r} + 0.1034 \quad (20)$$

<https://www.tytorobotics.com/pages/series-1580-1585>

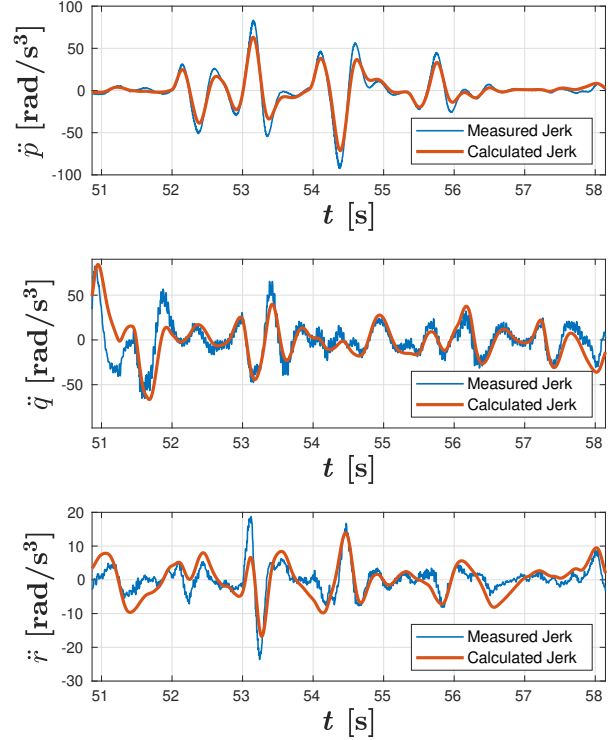


Fig. 7. Measured jerk responses versus those calculated using control derivatives.

Using the same apparatus as outlined in subsection III-B for the modelling of the actuator dynamics, the linear mapping between the servo PWM command and the angle in degrees was obtained and is given by the following equation.

$$\delta_{l,r} = 0.1096 \cdot \text{PWM} \quad (21)$$

#### IV. RESULTS

In order to test that using thrust vectoring as the only means of control moment generation in tailsitters is viable, a series of test flights were conducted. First, the analytical definition of the control effectiveness matrix was validated followed by the evaluation of the performance of the INDI controller's implementation.

##### A. Control Effectiveness Matrix

In order to verify that both the analytical definition of the control effectiveness matrix based on kinematics (Equation 8) as well as the modelling of the actuator dynamics hold true a number of vertical test flights were conducted. These test flights were conducted in an indoor arena limiting the chances of disturbances

allowing for the comparison of calculated jerk responses to measured jerk responses subject to the same actuator inputs sequence. The control derivatives of each actuator on each control DOF is calculated at 500 Hz based on the filtered actuator state of the previous time step meaning its accuracy is dependent on both the definition of the control derivatives and the accuracy of the modelled actuator state.

Figure 7 presents both measured and calculated roll, pitch and yaw jerk responses ( $\ddot{p}$ ,  $\ddot{q}$  &  $\ddot{r}$  respectively) to the same actuator input sequence from a segment of vertical flight. Examining jerk responses is convenient as the control effectiveness matrix  $\mathbf{G}$  maps increments in control inputs to jerks responses directly. One can see that the jerk responses calculated using the control derivatives generally follow the measured jerk responses. Peaks and troughs coincided along the time axis validating the parameters chosen for the modelling of the actuators. Discrepancies in magnitude can be attributed to a number of factors including: uncertainty in the mass moments of inertia  $\mathbf{I}$  used in calculating the control effectiveness matrix, discrepancies between the thrust calculated based on the static thrust test equation (Equation 20) and the actual thrust, discrepancies between the motor deflection angles  $\delta_{l,r}$  used for the calculation of the control effectiveness and the actual motor deflection angles, misalignment between the axis-system of the IMU and the actuators amongst other things.

### B. Performance of INDI Controller

Having verified that the actuator dynamics and the actuator control effectiveness have been sufficiently modelled, more extensive test flights focusing on the performance of the INDI controller outlined in section III will be discussed. A number of flights were conducted outdoors where transitions from vertical to horizontal flight were possible. The flight data presented in this section comes from two separate flights. Flight #1 had a duration of approximately 6 minutes. Additionally, a total of 8 transitions between the two flight phases were conducted during this flight, i.e. 4 from vertical to horizontal flight and 4 from horizontal to vertical flight. Flight #2 had a duration of approximately 2 minutes 10 seconds and a total of 3 transitions. This flight, though ultimately ending in a crash provides useful data from which conclusions can be drawn.

#### a) Flight #1:

In Figure 8(a), Figure 8(b) & Figure 8(c) depicting the roll  $\phi$ , pitch  $\theta$  and yaw  $\psi$  angle evolution for

TABLE IV  
MEAN ABSOLUTE ERROR BETWEEN THE COMMANDED ATTITUDE ANGLE AND THE MEASURED ATTITUDE ANGLE FOR OUTDOOR TEST FLIGHTS #1 & #2 TAKING INTO ACCOUNT THEIR RESPECTIVE TIME-DELAYS

		mean (abs (error)) [°]		
		Control DOF	Horizontal	Vertical
Flight #1	Roll $\phi$	3.23°	1.82°	2.86°
	Pitch $\theta$	2.34°	2.44°	2.34°
	Yaw $\psi$	1.47°	2.19°	1.65°
Flight #2	Roll $\phi$	3.42°	1.36°	2.83°
	Pitch $\theta$	3.43°	2.43°	2.98°
	Yaw $\psi$	2.65°	1.45°	2.19°

Flight #1, one can see that the implemented controller performs well at tracking commanded attitude angles in both horizontal and vertical flight. Though quite a lot of oscillations are visible from the figures, the mean absolute errors between the respective measured attitude angle and the commanded attitude angle over the entire flight are low. Table IV summarises the mean absolute errors for roll  $\phi$ , pitch  $\theta$  and yaw  $\psi$  for both Flights #1 and #2. For a fairer comparison of the two flights the cross-correlation of the measured and references signals was taken to estimate the time-delay  $\tau_d$  during the respective flights. The respective time-delays for Flight #1 and Flight #2 were 0.25s and 0.18s. From Table IV, for Flight #1, one can see that the poorest Euler angle tracking performance is roll  $\phi$  angle tracking during horizontal flight. Zooming into the roll  $\phi$  angle plot of Flight #1 for a portion of horizontal flight (see Figure 9) one can see that there is substantial overshoot and little to no damping suggesting that the gains  $K_\eta$  and  $K_\Omega$  for rotations around the  $Z_B$ -axis (roll  $\phi$  in horizontal flight) are not tuned correctly for horizontal flight. One can see from Table IV, for Flight #1, that yaw  $\psi$  tracking during vertical flight (rotations around the  $Z_B$ -axis) is a lot better. The aforementioned gains were tuned during indoor vertical flight tests which is reflected in the better performance of rotations around the  $Z_B$ -axis in vertical flight than in horizontal flight.

Also presented in Figure 8(d) are the actuator states as a percentage of their maximum states in the case of the motors and in degrees for tilts (maximum tilt deflection is 55°). It is noteworthy that during the entirety of the flight the only actuator to saturate is the left tilt  $\delta_l$ . Saturations of the left tilt occur three times for a total time of 0.544s (timestamps: [260.933, 261.095], [663.565, 263.767] & [307.033, 307.213]). Indicating that during piloted flight

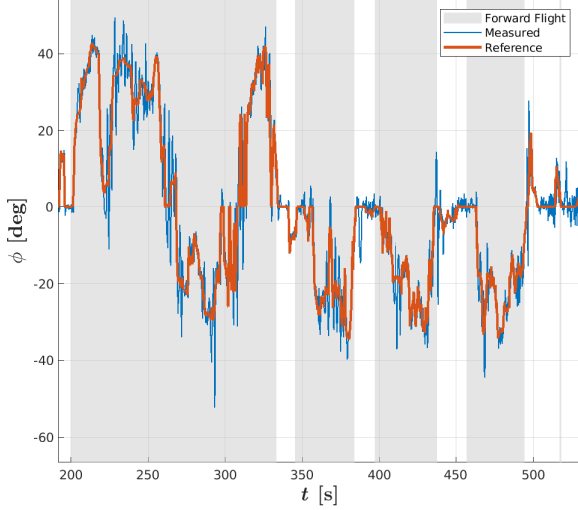
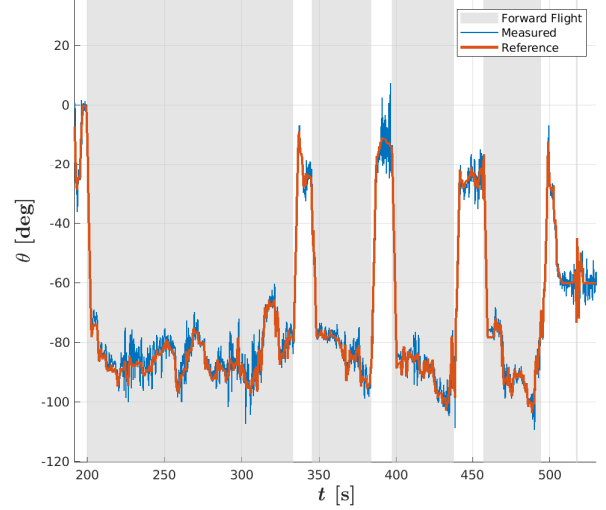
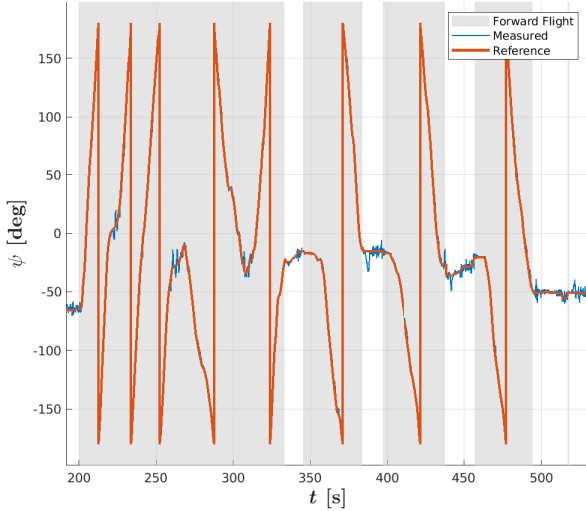
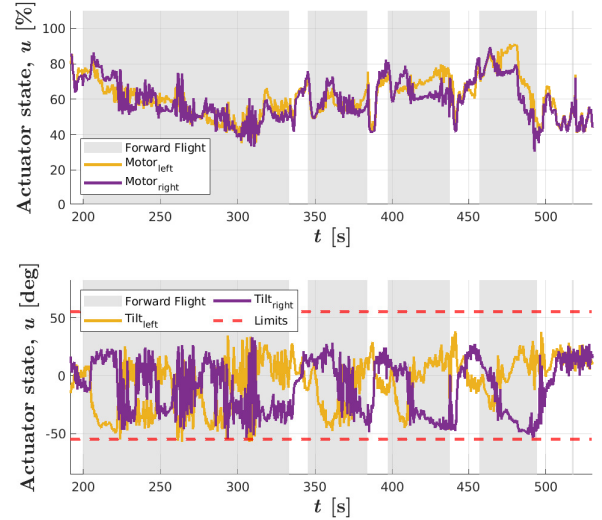
(a) Roll  $\phi$  measured and reference angles for the flight (ZXY Euler)(b) Pitch  $\theta$  measured and reference angles for the flight (ZXY Euler)(c) Yaw  $\psi$  measured and reference angles for the flight (ZXY Euler)(d) Evolution of actuator states  $u$ , (top) motor evolution as a percentage of max throttle setting, (bottom) tilt angle  $\delta_{l,r}$  in degrees, tilt limits of  $55^\circ$  also depicted

Fig. 8. Tracking performance of controller for Flight #1, grey shaded areas of all plots represent the horizontal phase of flight.

thrust vectoring alleviates actuator saturation.

Looking into the actuator deflections  $\delta_{l,r}$  versus the pitch  $\theta$  at points where the pitch angular acceleration  $\dot{q}$  is very low (equilibrium points) one can get more insight into the control authority of the tilts. Figure 11(a) presents the actuator states at various pitch angles with the following conditions simultaneously holding:  $-0.5 \leq \dot{q} \leq 0.5$  [deg/s<sup>2</sup>] and  $-5 \leq q \leq 5$  [deg/s]. These conditions were chosen such that a large enough spread of data points exist whilst still ensuring a relatively static equilibrium. One can see that there is one instance

of saturation (demarcated with a red diamond) for the left tilt with a value of  $-55$  deg. This point, however, corresponds to a left motor throttle setting of 43% which leaves an additional 57% unused throttle for a pitch moment contribution of the left-tilt-motor combination. At the point where the left tilt saturates the total pitch moment generated as a percentage of the available pitch moment should all actuators saturate is only -10.25% as depicted in Figure 11(b). This demonstrates that even during the saturation of one actuator, thrust vectoring provides significant pitch moment generation head room.

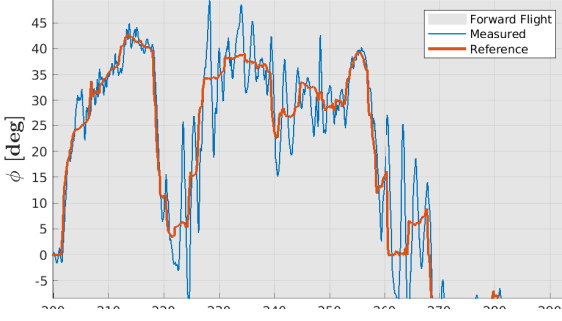


Fig. 9. Roll  $\phi$  measured and reference angles for Flight #1, zoomed in section of horizontal flight (ZXY Euler)

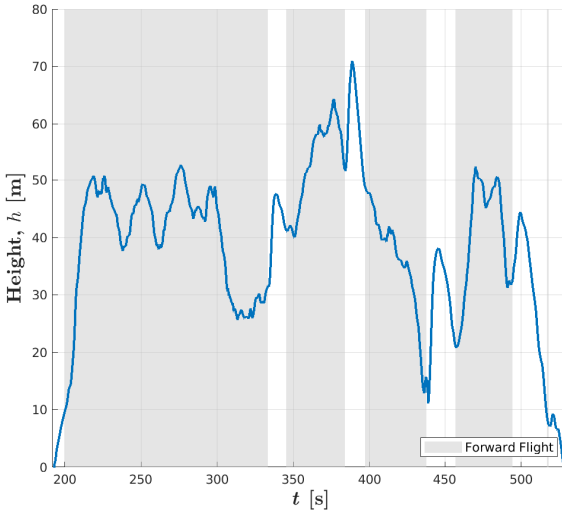


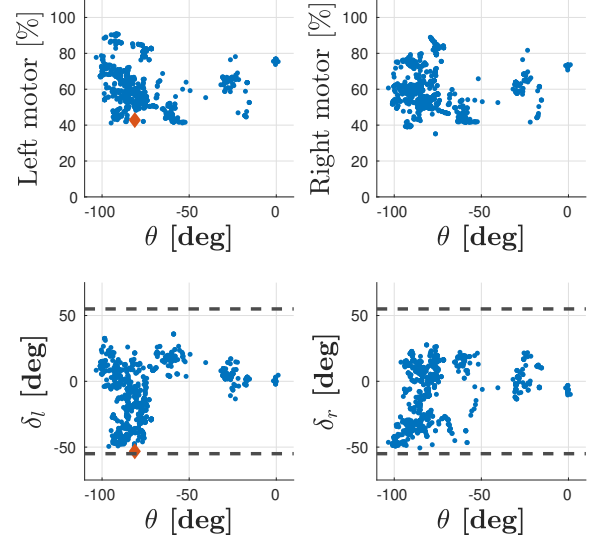
Fig. 10. Plot of the height evolution of the tailsitter over the course of Flight #1. Grey shaded areas of the plot indicate the horizontal phase of flight.

Also from Figure 11 one can see that large negative tilt deflections are often required to hold a pitch angle of around  $-90$  deg, i.e. during level flight.

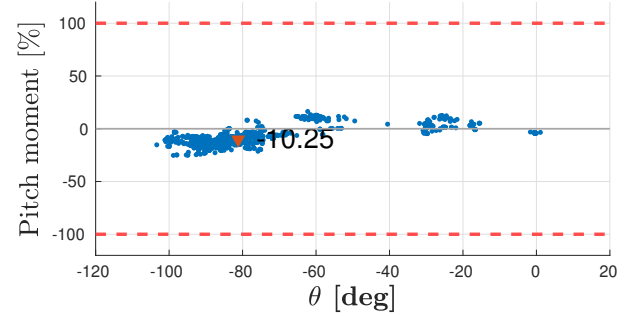
It is worth mentioning that the flight presented in this subsection was manually piloted making it difficult to limit the increase in altitude following the transition from horizontal back to vertical flight. This is clearly visible in Figure 10 where altitude gains of 16.0, 18.5, 23.1 and 11.0 m at timestamps ([333, 338], [383, 388], [437, 444] and [494, 498] respectively) follow the transitions from horizontal back to vertical flight.

### b) Flight #2:

From Figure 12(a), Figure 12(b) & Figure 12(c) one can see that the tracking performance of the Euler angles



(a) Tilt deflections  $\delta_{l,r}$  at varying pitch  $\theta$  angle equilibrium points



(b) Pitch control moment as percentage of total available pitch moment generation capability

Fig. 11. Illustration of pitch moment generation head room despite occurrence of saturation of left tilt (Flight #1)

throughout Flight #2 is generally improved except for a finite number of times when large oscillations take place on all three axes during forward flight. It is these large oscillations which ultimately caused the MAV to crash. For each of the four times that large unstable oscillations occur, roll  $\phi$  angle tracking degradation precedes that of the tracking of the remaining two Euler angles.

The main differences between Flight #1 and Flight #2 are changes in gains vectors  $K_\eta$  and  $K_\Omega$  and minor changes to the hyper parameters of the control effectiveness matrix  $\mathbf{G}$ . From Table IV one can see that across the board the tracking of the Euler angles in vertical flight has improved versus Flight #1. In horizontal flight the mean absolute errors are marginally worse despite being heavily skewed because of the extremely large oscillations starting at approximately 390s, 415s, 425s and 480s.

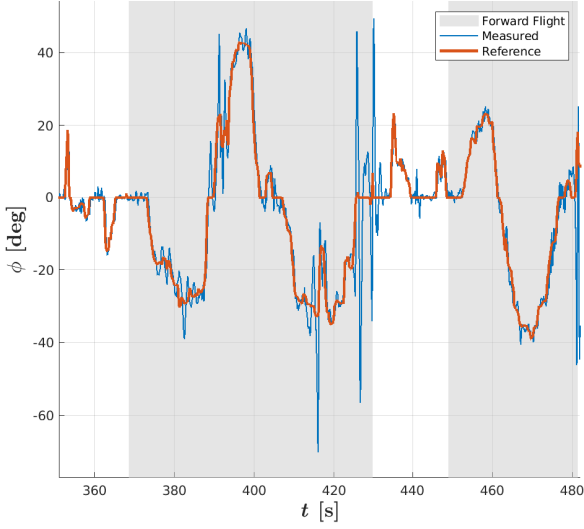
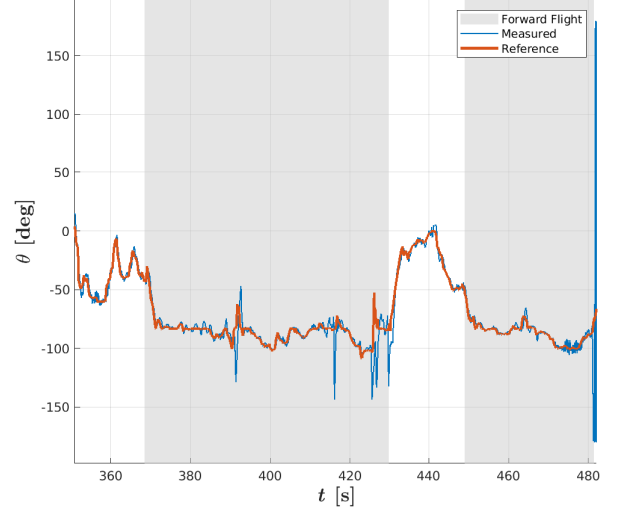
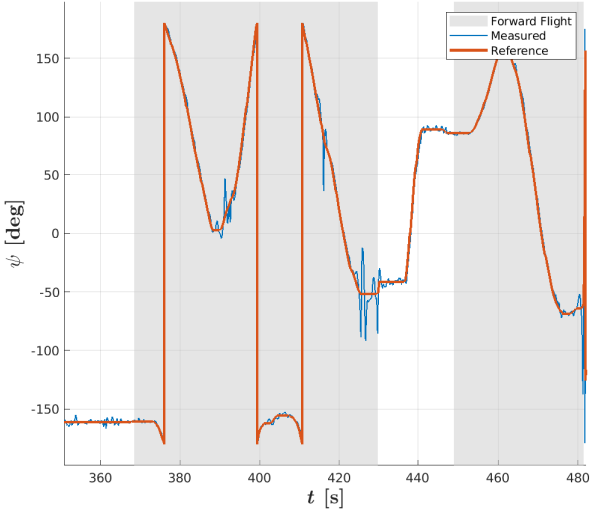
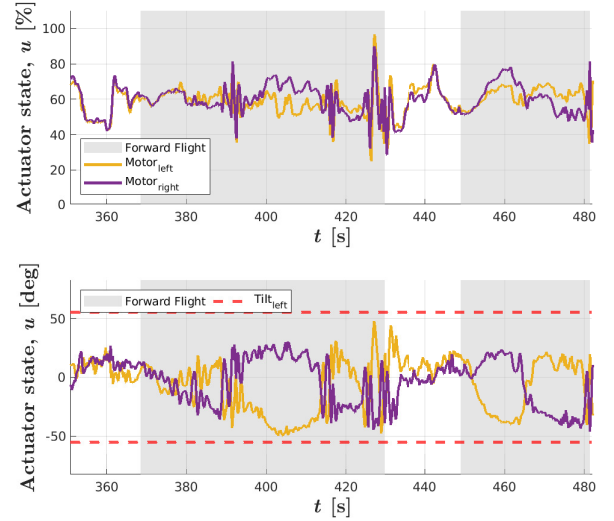
(a) Roll  $\phi$  measured and reference angles for the flight (ZXY Euler)(b) Pitch  $\theta$  measured and reference angles for the flight (ZXY Euler)(c) Yaw  $\psi$  measured and reference angles for the flight (ZXY Euler)(d) Evolution of actuator states  $u$ , (top) motor evolution as a percentage of max throttle setting, (bottom) tilt angle  $\delta_{l,r}$  in degrees, tilt limits of  $55^\circ$  also depicted

Fig. 12. Tracking performance of controller for Flight #2, grey shaded areas of all plots represent the horizontal phase of flight.

Furthermore, during this flight  $Y_B$ -accelerations were observed suggesting the presence of sideslip (see Figure 13). Sideslip degrades the lift of the wing affecting performance and could in part be contributing to the oscillatory behaviour in forward flight.

## V. DISCUSSION & RECOMMENDATIONS

Even though in section IV it was verified that the actuator dynamics and control effectiveness have been sufficiently modelled and the ability of the controller to track commanded attitude angles was demonstrated, little

can be said about to what extent the wing experiences stall. As introduced, tailsitters with conventional control surfaces for control moment generation struggle with actuator saturation especially during transition. During transition tailsitters experience flow separation over the wing meaning that for a portion of the transition of a conventional tailsitter a significant amount of the pitch  $\theta$  and yaw  $\psi$  moment generation falls on the prop-washed portion of the flaps. This is particularly a problem during the transition back to vertical flight as typically hybrids are designed for passive stability during horizontal flight -

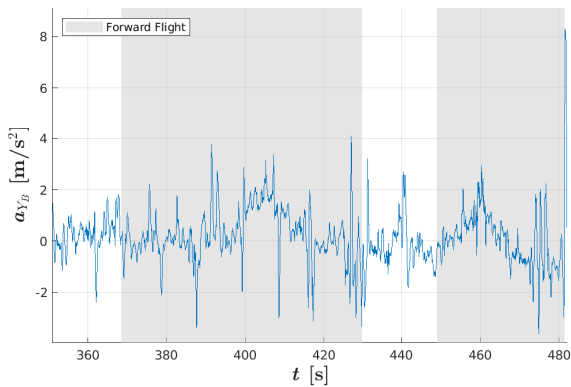


Fig. 13. Accelerometer measurements in the  $Y_B$  direction during Flight #2

the phase of flight constituting the greatest proportion of the flight duration. The pitch down tendency associated with passive stability means that greater pitch moment generation head room is desirable. In the case of the test flight results presented in section IV the large altitude gains following transition back to vertical flight indicate a significant velocity component in the negative  $Z_N$ -axis preventing the angle of attack from becoming too high and thus suppressing stall. In order to categorically demonstrate the superior control moment generation of thrust vectoring as implemented on this platform it is recommended that an altitude hold outer-loop controller is implemented. This would limit the magnitude of any velocity component in the negative  $Z_N$ -axis direction forcing stall. Given no actuator saturations, a stalled wing during transition from horizontal flight to vertical flight would allow one to declare the use of thrust vectoring for control moment generation as a viable option for alleviating actuator saturations in tailsitters.

Figure 11 shows two things that indicating that thrust vectoring may alleviate actuator saturations in tailsitters. First, that there was only one instance of tilt saturation whilst holding a static pitch angle over the duration of Flight #1. Secondly, there is sufficient head room for positive pitch moment generation (lots of head room for additional positive tilt deflections) indicating that this implementation of thrust vectoring could alleviate actuator saturation during transition from horizontal back to vertical flight. The fact that large negative deflections are present during level forward flight is worth discussing, however. The presence of large negative tilt deflections may indicate that the tailsitter was not passively stable in forward flight despite the c.o.g. being balanced to this end. From Figure 11(b) one can see that negative pitch moments are regularly commanded to hold a pitch angle

of approximately  $-90^\circ$ . Hybrid MAVs aim to expand mission capabilities with fast and efficient forward flight. The very efficiency gained by having a wing for aerodynamic lift is eroded by commanding large tilts and by extension requiring large increases in throttle. Future work may look into the addition of ailerons for  $Z_B$ -axis control during fast horizontal flight

As briefly noted in subsection IV-A, errors between the thrust calculated based on the static thrust equation (Equation 20) and the real thrust being output by the motor-propeller combination will in turn result in errors in the control effectiveness matrix  $G$ . Thrust force is generated through the change in momentum of the air flowing through the propeller disk. The difference between the static thrust  $T_0$  and the thrust in the presence of a non-zero inflow velocity is governed by the following relationship as adapted from [22]:

$$T_c = T_0 \cdot \frac{v_e - v}{v_e} \quad (22)$$

Where  $v_e$  is the exit velocity of the air through the propeller disk,  $v$  is the airspeed and the static thrust  $T_0$  is calculated using Equation 20. Assuming all energy is transferred from the propeller to the air, the exit velocity  $v_e$  can be estimated as follows:

$$v_e = \frac{\omega}{2\pi} \cdot PP \quad (23)$$

Where the propeller pitch  $PP$  in m is the displacement made for one complete revolution and  $\omega$  is the angular rate in rad/s. Figure 14 shows how the static thrust equation (Equation 20) changes with increasing airspeed. Should reliable airspeed data be available such corrections can be made making the calculated control effectiveness more accurate. This is recommended for future work.

In Flight #2 large rapid oscillations are observed 4 times during horizontal flight ultimately leading to a crash. Each period of oscillation begins with a degradation in roll angle tracking. This could be in part due to the presence of sideslip. As  $Y_B$  accelerations indicate the presence of sideslip, this measurement can be exploited to reduce the sideslip angle as done in [3]. Additionally, during horizontal flight, changes to the motor tilt angles changes the local angle of attack of the wing. The relationship between a change in motor tilt angle and the change in angle of attack of the wing in its wake is unknown and therefore its effect cannot be quantified. Large changes are undesirable however, and during horizontal flight the effectiveness of the thrust vectoring decreases due to the inflow velocity through the propeller disk as discussed above leading to

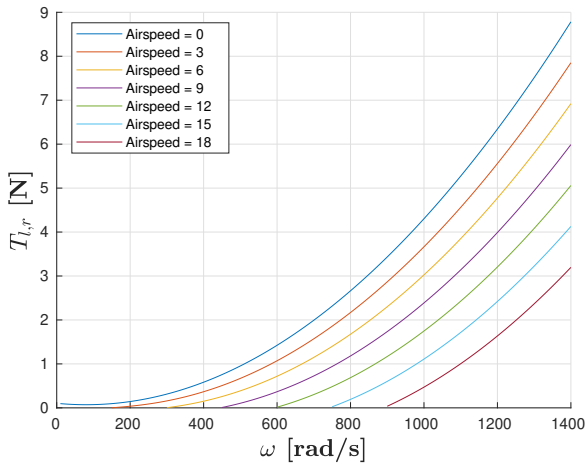


Fig. 14. Thrust as a function of angular rate  $\omega$  for different airspeeds

larger required deflections. The addition of ailerons for fast horizontal flight would eliminate this effect. Again, future work may look into the addition of ailerons to this end.

As mentioned in subsection III-C the control allocation algorithm used in this implementation is the WLS control allocation algorithm which makes use of the linearised actuator control effectiveness matrix presented in Equation 8. In the case of this tailsitter with nonlinear and highly coupled effectors the use of a linearised control effectiveness matrix results in an error between the calculated control moment increment and the required control moment increment. In this research constraining the control objective such that the calculated control moment increment remains in the vicinity of the linearisation point was opted for. Additional increments are required as a result should the control objective be too large. This adds delay. Future work may be to implement a nonlinear control allocation algorithm based on the equations of motion outlined in Equation 1.

Lastly, from Table IV a clear difference in performance between horizontal and forward flight is visible and generally performance is better in vertical flight. This is because gains and hyper parameters are tuned during indoor vertical flight. Implementing gain scheduling (perhaps even some sort of gain scaling with measured airspeed) would result in better performance.

## VI. CONCLUSION

In this paper a novel configuration of tailsitter MAV which exclusively uses thrust vectoring for the generation of control moments was presented. It features two motors mounted to two tilting mechanisms all mounted

forward of the leading edge. This configuration allows for the control derivatives to be calculated analytically for the implementation of incremental nonlinear dynamic inversion for attitude control. The INDI control law was detailed along with some of the concessions that had to be made in order for the successful implementation on the presented tailsitter. Satisfactory controller performance in tracking commanded attitude angles was demonstrated during test flights with the mean absolute errors between the commanded attitude angles and the measured angles being less than  $2.98^\circ$  over the entire flight envelope over the two presented flights involving multiple transitions. With this particular implementation of thrust vectoring for control moment generation it is demonstrated that over the entire flight envelope including multiple transitions commanded attitude angles can be tracked with minimal actuator saturations (a total time of 0.544s of saturation in one of the two flights documented in this paper). It cannot, however, be said categorically that in the presence of a completely stalled wing there remains sufficient control moment generation. This would require the demonstration of no actuator saturations whilst forcing the wing to stall. It is shown, however, that when looking at pitch angles versus tilt deflections during equilibrium there remains unused control authority. This paper demonstrates both the physical feasibility of exclusively using thrust vectoring in tailsitters as well as the adaptation of the INDI control law for the control of such tailsitters.

## REFERENCES

- [1] A. S. Saeed *et al.*, “A survey of hybrid Unmanned Aerial Vehicles,” *Progress in Aerospace Sciences*, vol. 98, no. December 2017, pp. 91–105, 2018. [Online]. Available: <https://doi.org/10.1016/j.paerosci.2018.03.007>
- [2] G. Flores, I. Lugo, and R. Lozano, “6-DOF hovering controller design of the Quad Tiltrotor aircraft: Simulations and experiments,” *Proceedings of the IEEE Conference on Decision and Control*, vol. 2015-Febru, no. February, pp. 6123–6128, 2014.
- [3] E. J. Smeur, M. Bronz, and G. C. de Croon, “Incremental control and guidance of hybrid aircraft applied to a tailsitter unmanned air vehicle,” *Journal of Guidance, Control, and Dynamics*, vol. 43, no. 2, pp. 274–287, 2020.
- [4] M. Bronz, “Comparison of pitching moment generation via flap deflection and thrust vectoring on a generic blown-wing model,” in *AIAA Aviation 2019 Forum*, 2019, p. 3171.
- [5] X. Lyu *et al.*, “Design and implementation of a quadrotor tailsitter VTOL UAV,” *Proceedings - IEEE International Conference on Robotics and Automation*, pp. 3924–3930, 2017.
- [6] X. Lyu *et al.*, “Disturbance Observer Based Hovering Control of Quadrotor Tail-Sitter VTOL UAVs Using  $H_\infty$  Synthesis,” *IEEE Robotics and Automation Letters*, vol. 3, no. 4, pp. 2910–2917, 2018.
- [7] A. Oosedo *et al.*, “Optimal transition from hovering to level-flight of a quadrotor tail-sitter UAV,” *Autonomous Robots*, vol. 41, no. 5, pp. 1143–1159, 2017.

- [8] T. Matsumoto *et al.*, “A hovering control strategy for a tail-sitter VTOL UAV that increases stability against large disturbance,” *Proceedings - IEEE International Conference on Robotics and Automation*, pp. 54–59, 2010.
- [9] J. L. Forshaw and V. J. Lappas, “High-fidelity modeling and control of a twin helicopter rotor tailsitter,” *AIAA Guidance, Navigation, and Control Conference 2011*, no. August, pp. 1–16, 2011.
- [10] L. R. Lustosa, F. Defay, and J. M. Moschetta, “Longitudinal study of a tilt-body vehicle: Modeling, control and stability analysis,” *2015 International Conference on Unmanned Aircraft Systems, ICUAS 2015*, pp. 816–824, 2015.
- [11] J. Zhong *et al.*, “L1 adaptive control of a dual-rotor tail-sitter unmanned aerial vehicle with input constraints during hover flight,” *IEEE Access*, vol. 7, pp. 51 312–51 328, 2019.
- [12] Y. Yang *et al.*, “Robust proportional incremental nonlinear dynamic inversion control of a flying-wing tailsitter,” *Proceedings of the Institution of Mechanical Engineers, Part G: Journal of Aerospace Engineering*, vol. 234, no. 16, pp. 2274–2295, 2020.
- [13] Y. Yang, J. Zhu, and J. Yang, “INDI-based transitional flight control and stability analysis of a tail-sitter UAV,” *IEEE Transactions on Systems, Man, and Cybernetics: Systems*, vol. 2020-October, pp. 1420–1426, 2020.
- [14] E. A. Tal and S. Karaman, “Global trajectory-tracking control for a tailsitter flying wing in agile uncoordinated flight,” in *AIAA AVIATION 2021 FORUM*, 2021, p. 3214.
- [15] S. Raab *et al.*, “Proposal of a unified control strategy for vertical take-off and landing transition aircraft configurations,” *2018 Applied Aerodynamics Conference*, 2018.
- [16] F. Binz, T. Islam, and D. Moormann, “Attitude control of tiltwing aircraft using a wing-fixed coordinate system and incremental nonlinear dynamic inversion,” *International Journal of Micro Air Vehicles*, vol. 11, 2019.
- [17] E. J. Smeur, Q. Chu, and G. C. de Croon, “Adaptive incremental nonlinear dynamic inversion for attitude control of micro aerial vehicles,” *2016 AIAA Guidance, Navigation, and Control Conference*, pp. 1–16, 2016.
- [18] E. J. Smeur, G. C. de Croon, and Q. Chu, “Cascaded incremental nonlinear dynamic inversion for MAV disturbance rejection,” *Control Engineering Practice*, vol. 73, no. January, pp. 79–90, 2018. [Online]. Available: <https://doi.org/10.1016/j.conengprac.2018.01.003>
- [19] A. Mancinelli *et al.*, “Dual-axis tilting rotor quad-plane design, simulation, flight and performance comparison with a conventional quad-plane design,” in *2022 International Conference on Unmanned Aircraft Systems (ICUAS)*, 2022, pp. 197–206.
- [20] G. C. Goodwin *et al.*, *Control system design*. Prentice Hall Upper Saddle River, 2001, vol. 240.
- [21] E. J. Smeur, E. C. Höppener, and D. Wagter, “Prioritized Control Allocation for Quadrotors Subject to Saturation,” *International Micro Air Vehicle Conference and Flight Competition 2017*, pp. 37–43, 2017.
- [22] V. Bertram, “Chapter 2 - propellers,” in *Practical Ship Hydrodynamics (Second Edition)*, second edition ed., V. Bertram, Ed. Oxford: Butterworth-Heinemann, 2012, pp. 41–72. [Online]. Available: <https://www.sciencedirect.com/science/article/pii/B9780080971506100028>

# 5

## Conclusion

Advancements in the capabilities of micro air vehicles along with improvements in reliability have seen them used for tasks which traditionally required significant human supervision, control and even physical effort. Hybrid MAVs feature a wing or wings for fast, efficient forward flight as well as being capable of hovering and vertical take-off and landing. This makes them particularly useful for applications like the inspection of infrastructure, the monitoring of crops, reconnaissance and surveillance. A general review of the hybrid MAV space found that hybrid MAVs can be divided into two main categories namely: Convertiplanes and Tail-sitters. The former having the advantage of offering an approximately level platform during all flight phases whilst the disadvantage of generally having one of more effectors inoperable regardless of phase of flight. Convertiplanes can be further split into a number of subcategories, tilt-rotors being a relevant subcategory to this research. Tail-sitters trade mechanical simplicity for increased complexity control-wise; they have the advantage of not requiring different effectors for vertical and horizontal flight but on the other hand must pitch  $90^\circ$  between horizontal and vertical flight.

The large flight envelope of hybrid MAVs means that they are inherently more difficult to control. The varied flight envelope (from low-speed vertical flight to fast horizontal flight) means that controllers have to deal with significantly different dynamics presented by each flight phase [4]. Robust control techniques are necessary to mitigate such issues. PID control, Optimal LQR control and INDI control have all been implemented for the control of Hybrid MAVs. PID controllers exploit no knowledge of the system itself however this is often times accompanied by less than adequate robustness to unknown disturbances unless augmented with some sort of adaptive controller. Optimal LQR controllers generate control inputs through calculating an optimal LQR selected gain based on the matrices of a state-space system thus making them more susceptible to model mismatches. It is noted by Forshaw et al. [20], however, that their LQR controller was more robust to deviations in the equations of motion than a PID controller controlling the same tail-sitter. INDI control is a lot more robust against unknown disturbances and uncertainties than PID control and LQR control. This is because it relies on (in many cases) inertial measurements and the system's control derivatives to incrementally update control inputs to achieve desired increments in system outputs. The control effectiveness and actuator dynamics (should actuator feedback not be available) are the only required pieces of knowledge for the implementation of this controller. The control effectiveness matrices were derived from test flight data in [1], CFD modelling in the cases of [9] and [16], mathematical modelling in the cases of [11] and [31] and numerical differentiation of a plant model in [8]. Tal et al. [18] implement INDI control in a completely different way which does not involve linearisation of dynamics for inversion. Instead they makes use of an simplified  $\phi$ -theory aerodynamic forces and moments model to derive expressions for control inputs and states in terms of flat outputs allowing for fully nonlinear inversion (thus without requiring linearisation).

In a parallel research thread, issues surrounding the loss of control moment generation as a result of actuator saturation or flow separation during stalled flight was conducted. Collective thrust transitioning tail-sitters with a total of 4 effectors (namely 2 rotors and 2 flaps) inevitably have coupled effectors further diminishing the control authority available for the control of each separate control DOF. Actuator saturation was reported or alluded to in [1], [2], [16], [17] and [19] (tail-sitters) and [6] and [8] (tilt-rotors). Bronz [2] found that thrust vectoring could provide almost 2 times the control moment generation versus flap deflection and proposed thrust vectoring as a means to combat actuator saturation and loss of control moment generation.

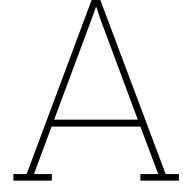
It was found that a research gap lies where INDI control of a tail-sitter MAV and thrust vectoring as a means of control moment generation intersect. This research gap was filled by investigating, designing (and building) and experimenting with the control of a tail-sitter MAV with a pair of tiltable propellers serving as its only effectors. INDI control was implemented for attitude control and the control moment derivatives were formulated analytically from kinematic equations. Satisfactory controller performance in tracking commanded attitude angles was demonstrated during test flights with the mean absolute errors between the commanded attitude angles and the measured angles being less than  $2.98^\circ$  over the entire flight envelope over the two presented flights involving multiple transitions. With this particular implementation of thrust vectoring for control moment generation it is demonstrated that over the entire flight envelope including multiple transitions commanded attitude angles can be tracked with minimal actuator saturations (a total time of 0.544s of saturation in one of the two flights documented in this paper). It cannot, however, be said categorically that in the presence of a completely stalled wing there remains sufficient control moment generation. This would require the demonstration of no actuator saturations whilst forcing the wing to stall. It is shown, however, that when looking at pitch angles versus tilt deflections during equilibrium there remains unused control authority. This research demonstrates both the physical feasibility of exclusively using thrust vectoring in tailsitters as well as the adaptation of the INDI control law for the control of such tailsitters. It was, however noticed that at time during horizontal flight, large tilt deflections were present. Hybrid MAVs aim to expand mission capabilities with fast and efficient forward flight. The very efficiency gained by having a wing for aerodynamic lift is eroded by commanding large tilts and by extension requiring large increases in throttle. Future work may look into the addition of ailerons for  $Z_B$ -axis control during fast horizontal flight. Lastly, using tilting, leading edge mounted propellers has the added bonus of allowing the experimental platform to hinge up and down about its trailing edge for take-off and landing. This has the benefit of improving reliability of take-offs and landings in adverse flying conditions. Take-offs and landings were successfully performed in this manner.

# References

- [1] Ewoud J.J. Smeur, Murat Bronz, and Guido C.H.E. de Croon. “Incremental control and guidance of hybrid aircraft applied to a tailsitter unmanned air vehicle”. In: *Journal of Guidance, Control, and Dynamics* 43.2 (2020), pp. 274–287. ISSN: 15333884. DOI: 10.2514/1.G004520.
- [2] Murat Bronz. “Comparison of Pitching Moment Generation via Flap Deflection and Thrust Vectoring on A Generic Blown-Wing Model”. In: June (2019), pp. 1–12. DOI: 10.2514/6.2019-3171.
- [3] Adnan S. Saeed et al. “A survey of hybrid Unmanned Aerial Vehicles”. In: *Progress in Aerospace Sciences* 98.December 2017 (2018), pp. 91–105. ISSN: 03760421. DOI: 10.1016/j.paerosci.2018.03.007. URL: <https://doi.org/10.1016/j.paerosci.2018.03.007>.
- [4] Gerardo Flores, Israel Lugo, and Rogelio Lozano. “6-DOF hovering controller design of the Quad Tiltrotor aircraft: Simulations and experiments”. In: *Proceedings of the IEEE Conference on Decision and Control* 2015-Febru.February (2014), pp. 6123–6128. ISSN: 07431546. DOI: 10.1109/CDC.2014.7040348.
- [5] Dawei Wu, Hanbing Li, and Shu Li. “Flight dynamics study of a small tilt rotor UAV with tail propeller”. In: *16th AIAA Aviation Technology, Integration, and Operations Conference* June (2016). DOI: 10.2514/6.2016-3450.
- [6] Gabriele Di Francesco, Egidio D’Amato, and Massimiliano Mattei. “Incremental nonlinear dynamic inversion and control allocation for a tilt rotor UAV”. In: *AIAA Guidance, Navigation, and Control Conference* January (2014), pp. 1–29. DOI: 10.2514/6.2014-0963.
- [7] Gabriele Di Francesco, Egi D’Amato, and Massimiliano Mattei. “INDI control with direct lift for a tilt rotor UAV”. In: *IFAC-PapersOnLine* 28.9 (2015), pp. 156–161. ISSN: 24058963. DOI: 10.1016/j.ifacol.2015.08.076. URL: <http://dx.doi.org/10.1016/j.ifacol.2015.08.076>.
- [8] Stefan Raab et al. “Proposal of a unified control strategy for vertical take-off and landing transition aircraft configurations”. In: *2018 Applied Aerodynamics Conference* (2018). DOI: 10.2514/6.2018-3478.
- [9] Zhenchang Liu et al. “VTOL UAV transition maneuver using incremental nonlinear dynamic inversion”. In: *International Journal of Aerospace Engineering* 2018 (2018). ISSN: 16875974. DOI: 10.1155/2018/6315856.
- [10] Haowei Gu et al. “Development and experimental verification of a hybrid vertical take-off and landing (VTOL) unmanned aerial vehicle(UAV)”. In: *2017 International Conference on Unmanned Aircraft Systems, ICUAS 2017* (2017), pp. 160–169. DOI: 10.1109/ICUAS.2017.7991420.
- [11] F. Binz, T. Islam, and D. Moormann. “Attitude control of tiltwing aircraft using a wing-fixed coordinate system and incremental nonlinear dynamic inversion”. In: *International Journal of Micro Air Vehicles* 11 (2019). ISSN: 17568307. DOI: 10.1177/1756829319861370.

- [12] Philipp Hartmann, Carsten Meyer, and Dieter Moormann. “Unified velocity control and flight state transition of unmanned tilt-wing aircraft”. In: *Journal of Guidance, Control, and Dynamics* 40.6 (2017), pp. 1348–1359. ISSN: 15333884. DOI: 10.2514/1.G002168.
- [13] Robin Hill Zamri Omar, Cees Bil. “The Development of A New VTOL UAV Configuration For Law Enforcement”. In: *2008 International Conference on Mechanical & Manufacturing Engineering* May (2008), pp. 21–23. DOI: 97-98-2963-59-2.
- [14] Matthew E. Argyle, Randal W. Beard, and Stephen Morris. “The Vertical Bat tail-sitter: Dynamic model and control architecture”. In: *Proceedings of the American Control Conference* (2013), pp. 806–811. ISSN: 07431619. DOI: 10.1109/acc.2013.6579935.
- [15] Yeunduk Jung and David Hyunchul Shim. “Development and application of controller for transition flight of tail-sitter UAV”. In: *Journal of Intelligent and Robotic Systems: Theory and Applications* 65.1-4 (2012), pp. 137–152. ISSN: 09210296. DOI: 10.1007/s10846-011-9585-1.
- [16] Yunjie Yang et al. “Robust proportional incremental nonlinear dynamic inversion control of a flying-wing tailsitter”. In: *Proceedings of the Institution of Mechanical Engineers, Part G: Journal of Aerospace Engineering* 234.16 (2020), pp. 2274–2295. ISSN: 20413025. DOI: 10.1177/0954410020926657.
- [17] Jingyang Zhong et al. “L1 adaptive control of a dual-rotor tail-sitter unmanned aerial vehicle with input constraints during hover flight”. In: *IEEE Access* 7 (2019), pp. 51312–51328. ISSN: 21693536. DOI: 10.1109/ACCESS.2019.2911897.
- [18] Ezra A. Tal and Sertac Karaman. “Global Trajectory-tracking Control for a Tailsitter Flying Wing in Agile Uncoordinated Flight”. In: (2021). DOI: 10.2514/6.2021-3214.
- [19] Jason L. Forshaw, Vaios J. Lappas, and Phil Briggs. “Transitional control architecture and methodology for a twin rotor tailsitter”. In: *Journal of Guidance, Control, and Dynamics* 37.4 (2014), pp. 1289–1298. ISSN: 15333884. DOI: 10.2514/1.G000314.
- [20] Jason L. Forshaw and Vaios J. Lappas. “High-fidelity modeling and control of a twin helicopter rotor tailsitter”. In: *AIAA Guidance, Navigation, and Control Conference 2011* August (2011), pp. 1–16. DOI: 10.2514/6.2011-6637.
- [21] C. De Wagter et al. “The NederDrone: A hybrid lift, hybrid energy hydrogen UAV”. In: *International Journal of Hydrogen Energy* 46.29 (2021), pp. 16003–16018. ISSN: 03603199. DOI: 10.1016/j.ijhydene.2021.02.053. arXiv: 2011.03991.
- [22] Atsushi Oosedo et al. “Optimal transition from hovering to level-flight of a quadrotor tail-sitter UAV”. In: *Autonomous Robots* 41.5 (2017), pp. 1143–1159. ISSN: 15737527. DOI: 10.1007/s10514-016-9599-4.
- [23] Ximin Lyu et al. “Design and implementation of a quadrotor tail-sitter VTOL UAV”. In: *Proceedings - IEEE International Conference on Robotics and Automation* (2017), pp. 3924–3930. ISSN: 10504729. DOI: 10.1109/ICRA.2017.7989452.
- [24] Pranay Sinha et al. “Versatile, modular, extensible VTOL aerial platform with autonomous flight mode transitions”. In: *IEEE Aerospace Conference Proceedings* (2012). ISSN: 1095323X. DOI: 10.1109/AERO.2012.6187313.
- [25] Ewoud J.J. Smeur, Guido C.H.E. De Croon, and Qiping Chu. “Gust disturbance alleviation with incremental nonlinear dynamic inversion”. In: *IEEE International Conference on Intelligent Robots and Systems 2016-Novem* (2016), pp. 5626–5631. ISSN: 21530866. DOI: 10.1109/IRoS.2016.7759827.
- [26] Takaaki Matsumoto et al. “A hovering control strategy for a tail-sitter VTOL UAV that increases stability against large disturbance”. In: *Proceedings - IEEE International Conference on Robotics and Automation* (2010), pp. 54–59. ISSN: 10504729. DOI: 10.1109/ROBOT.2010.5509183.

- [27] M. V. Khlebnikov and P. S. Shcherbakov. “Linear Quadratic Regulator: II. Robust Formulations”. In: *Automation and Remote Control* 80.10 (2019), pp. 1847–1860. ISSN: 16083032. DOI: 10.1134/S0005117919100060.
- [28] Leandro R. Lustosa, Francois Defay, and Jean Marc Moschetta. “Longitudinal study of a tilt-body vehicle: Modeling, control and stability analysis”. In: *2015 International Conference on Unmanned Aircraft Systems, ICUAS 2015* (2015), pp. 816–824. DOI: 10.1109/ICUAS.2015.7152366.
- [29] Jean-Jacques E. Slotine and Weiping Li. *Applied Nonlinear Control*. 1991. ISBN: 0130408905.
- [30] B. Paul Acquatella et al. “Robust nonlinear spacecraft attitude control using incremental nonlinear dynamic inversion”. In: *AIAA Guidance, Navigation, and Control Conference 2012* August (2012). DOI: 10.2514/6.2012-4623.
- [31] Ewoud J.J. Smeur, Qiping Chu, and Guido C.H.E. de Croon. “Adaptive incremental nonlinear dynamic inversion for attitude control of micro aerial vehicles”. In: *2016 AIAA Guidance, Navigation, and Control Conference* (2016), pp. 1–16. DOI: 10.2514/6.2016-1390.
- [32] Boyang Li et al. “Development of model predictive controller for a tail-sitter VTOL UAV in hover flight”. In: *Sensors (Switzerland)* 18.9 (2018), pp. 1–21. ISSN: 14248220. DOI: 10.3390/s18092859.
- [33] E. J.J. Smeur, E C Höppener, and D Wagter. “Prioritized Control Allocation for Quadrotors Subject to Saturation”. In: *International Micro Air Vehicle Conference and Flight Competition 2017* (2017), pp. 37–43.
- [34] Sergio Garcia-Nieto et al. “Motion equations and attitude control in the vertical flight of a VTOL bi-rotor UAV”. In: *Electronics (Switzerland)* 8.2 (2019), pp. 1–22. ISSN: 20799292. DOI: 10.3390/electronics8020208.



# Appendix

## A.1 Attitude Control

INDI for attitude control rests on the notion that all moments acting on a rigid body, both internally and externally produce the angular accelerations of the said body which, conveniently, can be derived from gyroscope measurements. Beginning with Euler's rotation equation which is given by Equation A.1 and expresses the total moments acting on a body in terms of the angular acceleration. This total moments can be expressed as the sum of a number of constituent components.

$$\begin{aligned} \mathbf{I}\dot{\boldsymbol{\Omega}} + \boldsymbol{\Omega} \times \mathbf{I}\boldsymbol{\Omega} &= \mathbf{M}_{\text{tot}} \\ \mathbf{I}\dot{\boldsymbol{\Omega}} + \boldsymbol{\Omega} \times \mathbf{I}\boldsymbol{\Omega} &= \mathbf{M}_c(\boldsymbol{\omega}, \boldsymbol{\delta}) + \mathbf{M}_a(\boldsymbol{\Omega}, \mathbf{v}_B) \end{aligned} \quad (\text{A.1})$$

Where  $\mathbf{M}_a$  is the vector of moments as a result of aerodynamic effects of the airframe and is therefore a function of the angular rates  $\boldsymbol{\Omega}$  and the body velocity  $\mathbf{v}_B$  and finally, the control moment  $\mathbf{M}_c$  is function of the angular rates of the motors  $\boldsymbol{\omega}$  and the tilt angle of the left and right motors  $\delta_{m_l}$  and  $\delta_{m_r}$  respectively and is given by the following equation.

$$\mathbf{M}_c = \begin{bmatrix} L \\ M \\ N \end{bmatrix} = \begin{bmatrix} -T_r b \cos \delta_{m_r} + T_l b \cos \delta_{m_l} \\ T_r l \sin \delta_{m_r} + T_l l \sin \delta_{m_l} \\ T_r b \sin \delta_{m_r} - T_l b \sin \delta_{m_l} \end{bmatrix} \quad (\text{A.2})$$

Where  $T_l$  and  $T_r$  are the thrust of the left and right motors respectively and are functions of the angular velocity  $\omega$  of each motors. Additionally  $\delta_{m_l}$  and  $\delta_{m_r}$  are defined as in Figure 4.1a.

Having rearranged Equation A.1 into the expression below (Equation A.3) one can take the first-order Taylor series expansion.

$$\dot{\boldsymbol{\Omega}} = \mathbf{I}^{-1} (\mathbf{M}_a(\boldsymbol{\Omega}, \mathbf{v}_B) - \boldsymbol{\Omega} \times \mathbf{I}\boldsymbol{\Omega}) + \mathbf{I}^{-1} \mathbf{M}_c(\boldsymbol{\omega}, \boldsymbol{\delta}_m) \quad (\text{A.3})$$

Where the first term encompasses the moments independent of the actuators. The Taylor expansion then simplifies to the expression given in Equation A.4 after grouping the terms evaluated at the current rates and inputs into the current angular acceleration  $\dot{\boldsymbol{\Omega}}_0$ . Note that the simplifying assumption that the partial derivatives w.r.t. the  $\boldsymbol{\Omega}$  and  $\mathbf{v}_B$  have a far smaller effect than the partial derivatives w.r.t.  $\boldsymbol{\omega}$ ,  $\dot{\boldsymbol{\omega}}$  and  $\boldsymbol{\delta}_e$  means than the remaining terms that need to be known for the implementation of INDI control only depend on the actuators. dropping higher order terms and making a few simplifications, invert the resulting equality to arrive at the INDI control law.

$$\begin{aligned} \dot{\boldsymbol{\Omega}} = \dot{\boldsymbol{\Omega}}_0 + \frac{\partial}{\partial \boldsymbol{\omega}} (I^{-1} \mathbf{M}_c(\boldsymbol{\omega}, \boldsymbol{\delta}_{e_0})) \Big|_{\boldsymbol{\omega}=\boldsymbol{\omega}_0} (\boldsymbol{\omega} - \boldsymbol{\omega}_0) \\ + \frac{\partial}{\partial \boldsymbol{\delta}_e} (I^{-1} \mathbf{M}_c(\boldsymbol{\omega}_0, \boldsymbol{\delta}_e)) \Big|_{\boldsymbol{\delta}=\boldsymbol{\delta}_0} (\boldsymbol{\delta}_e - \boldsymbol{\delta}_{e_0}) \end{aligned} \quad (\text{A.4})$$

For simplicity's sake the above equation can be expressed as in Equation A.5 below.

$$\dot{\boldsymbol{\Omega}} = \dot{\boldsymbol{\Omega}}_0 + \mathbf{G}(\mathbf{u} - \mathbf{u}_0) \quad (\text{A.5})$$

Where the subscript '0' indicates the current time or a time in the past and the control effectiveness matrix  $\mathbf{G}$  is comprised of an effectiveness value for each actuator on each controlled axis, i.e. comprised of effectiveness values  $G_{jk}$  which represent the effectiveness of actuator  $k$  on axis  $j$ . Equation A.5 can simply be inverted to obtain the INDI control law and is given by Equation A.6 (note that this equation resembles Equation 2.16).

$$\mathbf{u} = \mathbf{u}_0 + \mathbf{G}^{-1} (\mathbf{v} - \dot{\boldsymbol{\Omega}}_0) \quad (\text{A.6})$$

Where  $\mathbf{u}_0$  and  $\dot{\boldsymbol{\Omega}}_0$  the current control input vector and the measured angular acceleration vector respectively and  $\mathbf{v}$  a vector of virtual commands (the commanded angular acceleration)

## A.2 Velocity Control

Similarly to INDI for attitude control, INDI for velocity control rests on the notion that all forces acting on a body both internally and externally produce the linear accelerations that can simply be measured with accelerometers. The control law will be developed starting from Newton's second law applied to a hybrid MAV rearranged such that the second derivative of the position vector  $\ddot{\boldsymbol{\xi}}$  stands alone on the LHS of the equation. Note that these accelerations are in the NED frame, indicated by forces in the NED frame.

$$\ddot{\boldsymbol{\xi}} = \mathbf{g} + \frac{1}{m} \mathbf{L}_N(\boldsymbol{\eta}, V) + \frac{1}{m} \mathbf{D}_N(\boldsymbol{\eta}, V) + \frac{1}{m} \mathbf{T}_N(\boldsymbol{\eta}, \mathbf{T}_B) \quad (\text{A.7})$$

Where  $\mathbf{g}$  is the gravity vector,  $m$  the mass of the MAV,  $\mathbf{L}_N(\boldsymbol{\eta}, V)$  and  $\mathbf{D}_N(\boldsymbol{\eta}, V)$  the lift and drag vectors respectively both as functions of the attitude  $\boldsymbol{\eta}$  and airspeed  $V$  and  $\mathbf{T}_N(\boldsymbol{\eta}, \mathbf{T}_B)$  the thrust vector in the NED frame as a function of both attitude  $\boldsymbol{\eta}$  and the thrust in the body frame. In the case of the configuration outlined in Chapter 4 the thrust vector in the NED frame  $\mathbf{T}_N$  is a function of a thrust vector in the body frame  $\mathbf{T}_B$  which in turn is a function of both the thrust level  $T$  of each motor and an angular relationship between the motors and the MAV given by an vector of angles denoted by  $\boldsymbol{\delta}_m$ .

The elements of the above equation can be transformed from the body axes to the NED frame using Euler's ZXY rotation sequence. The following rotation matrix achieves this:

$$\mathbf{M}_{NB} = \begin{bmatrix} c\theta c\psi - s\phi s\theta s\psi & -c\phi s\psi & s\theta c\psi + s\phi c\theta s\psi \\ c\theta s\psi + s\phi s\theta c\psi & c\phi c\psi & s\theta s\psi - s\phi c\theta c\psi \\ -c\phi s\theta & s\phi & c\phi c\theta \end{bmatrix} \quad (\text{A.8})$$

Where 's' and 'c' represent sine and cosine respectively. The thrust vector in the NED frame  $\mathbf{T}_N$  can be obtained by simply multiplying the thrust vector in the body frame  $\mathbf{T}_B$  with the above transformation matrix. In the case of the experimental platform outlined in Chapter 4 the motors only tilt about an axis parallel with the  $Y_B$ -axis meaning there is no resulting force along the  $Y_B$ -axis (i.e.  $\mathbf{T}_B(\boldsymbol{\delta}_m, T) = [T_{X_B} \ 0 \ T_{Z_B}]^T$ ).  $\mathbf{T}_N$  is given by Equation A.9.

$$\mathbf{T}_N = \mathbf{M}_{NB} \begin{bmatrix} 0 \\ 0 \\ T_{Z_B} \end{bmatrix} = \begin{bmatrix} (s\theta c\psi + s\phi c\theta s\psi)T_{Z_B} \\ (s\theta s\psi - s\phi c\theta c\psi)T_{Z_B} \\ c\phi c\theta T_{Z_B} \end{bmatrix} \quad (\text{A.9})$$

Additionally, the lift vector is defined as being perpendicular to the airspeed vector and if the assumption is made that the sideslip angle  $\beta$  is small as well as the flight path angle being small then the lift vector is rotated from the vertical axis only by the roll angle  $\phi$ . The lift vector in the NED frame  $\mathbf{L}_N$  can simply be obtained by pre-multiplying  $\mathbf{L}_B$  with the rotation matrix with the pitch angle forced to zero,  $\mathbf{M}_{NB}^{\theta=0}$ . The same assumptions applies to drag and so the drag vector in the NED frame  $\mathbf{D}_N$  can be obtained in the same manner. Both  $\mathbf{L}_N$  and  $\mathbf{D}_N$  are given in Equations A.10 and A.11 respectively.

$$\mathbf{L}_N = \mathbf{M}_{NB}^{\theta=0} \mathbf{L}_B(\theta, V) = \begin{bmatrix} s\phi s\psi L(\theta, V) \\ -s\phi c\psi L(\theta, V) \\ c\phi L(\theta, V) \end{bmatrix} \quad \mathbf{D}_N = \mathbf{M}_{NB}^{\theta=0} \mathbf{D}_B(\theta, V) = \begin{bmatrix} c\psi D(\theta, V) \\ s\psi D(\theta, V) \\ 0 \end{bmatrix} \quad (\text{A.10}) \quad (\text{A.11})$$

A first-order Taylor expansion of Equation A.7 approximates the linear acceleration  $\ddot{\boldsymbol{\xi}}$  about a current point and is given by the following equation.

$$\begin{aligned} \ddot{\boldsymbol{\xi}} \simeq & \mathbf{g} + \frac{1}{m} \mathbf{L}_N(\boldsymbol{\eta}_0, V_0) + \frac{1}{m} \mathbf{D}_N(\boldsymbol{\eta}_0, V_0) + \frac{1}{m} \mathbf{T}_N(\boldsymbol{\eta}_0, T_0) + \frac{1}{m} \mathbf{L}_{N_\phi}(\phi, \theta_0, \psi_0, V_0) \Big|_{\phi=\phi_0} (\phi - \phi_0) \\ & + \frac{1}{m} \mathbf{L}_{N_\theta}(\phi_0, \theta, \psi_0, V_0) \Big|_{\theta=\theta_0} (\theta - \theta_0) + \frac{1}{m} \mathbf{L}_{N_\psi}(\phi_0, \theta_0, \psi, V_0) \Big|_{\psi=\psi_0} (\psi - \psi_0) \\ & + \frac{1}{m} \mathbf{L}_{N_V}(\phi_0, \theta_0, \psi_0, V) \Big|_{V=V_0} (V - V_0) + \frac{1}{m} \mathbf{D}_{N_\theta}(\theta, \psi_0, V_0) \Big|_{\theta=\theta_0} (\theta - \theta_0) \\ & + \frac{1}{m} \mathbf{D}_{N_\psi}(\theta_0, \psi, V_0) \Big|_{\psi=\psi_0} (\psi - \psi_0) + \frac{1}{m} \mathbf{D}_{N_V}(\theta_0, \psi_0, V) \Big|_{V=V_0} (V - V_0) \\ & + \frac{1}{m} \mathbf{T}_{N_\phi}(\phi, \theta_0, \psi_0, T_0) \Big|_{\phi=\phi_0} (\phi - \phi_0) + \frac{1}{m} \mathbf{T}_{N_\theta}(\phi_0, \theta, \psi_0, T_0) \Big|_{\theta=\theta_0} (\theta - \theta_0) \\ & + \frac{1}{m} \mathbf{T}_{N_\psi}(\phi_0, \theta_0, \psi, T_0) \Big|_{\psi=\psi_0} (\psi - \psi_0) + \frac{1}{m} \mathbf{T}_{N_{T_B}}(\phi_0, \theta_0, \psi_0, \mathbf{T}_B) \Big|_{\mathbf{T}_B=\mathbf{T}_{B,0}} (\mathbf{T}_B - \mathbf{T}_{B,0}) \end{aligned} \quad (\text{A.12})$$

Where the sub-subscripts represent the partial derivatives w.r.t. to that sub-subscript. The first 4 terms simply equate to the current linear acceleration  $\ddot{\boldsymbol{\xi}}_0$  and represents all the forces currently acting on the MAV and can be obtained by adding the gravity vector to the measured accelerations translated into the NED frame.

$$\ddot{\boldsymbol{\xi}}_0 \equiv \mathbf{g} + \frac{1}{m} \mathbf{L}_N(\boldsymbol{\eta}_0, V_0) + \frac{1}{m} \mathbf{D}_N(\boldsymbol{\eta}_0, V_0) + \frac{1}{m} \mathbf{T}_N(\boldsymbol{\eta}_0, T_0) \quad (\text{A.13})$$

The other terms in Equation A.12 represent the changes to the sum of all current forces as a result of changes in attitude, thrust and velocity. Equation A.12 can be further simplified if one assumes that the changes in drag are negligible compared to those of thrust and lift and can therefore be dropped. Additionally, if one assumes that yaw  $\psi$  cannot be commanded as it is being used for sideslip control meaning terms related to  $\psi$  can also be dropped. This simplifications result in the following equality.

$$\ddot{\boldsymbol{\xi}} = \ddot{\boldsymbol{\xi}}_0 + \frac{1}{m} (G_{L_N}(\boldsymbol{\eta}, V) + G_{T_N}(\boldsymbol{\eta}, \mathbf{T}_B)) (\mathbf{v} - \mathbf{v}_0) \quad (\text{A.14})$$

Where  $\mathbf{v} = [\phi \ \theta \ \mathbf{T}_B]^\top$  and the matrices of control derivatives  $G_{L_N}(\boldsymbol{\eta}, V)$  and  $G_{T_N}(\boldsymbol{\eta}, \mathbf{T}_B)$  are given by the following two equations.

$$G_{L_N}(\boldsymbol{\eta}, V) = \left[ \begin{array}{c} \left[ \mathbf{L}_{N_\phi}(\phi, \theta_0, \psi_0, V_0) \Big|_{\phi=\phi_0} \right]^\top \\ \left[ \mathbf{L}_{N_\theta}(\phi_0, \theta, \psi_0, V_0) \Big|_{\theta=\theta_0} \right]^\top \\ [\mathbf{0}_3]^\top \end{array} \right]^\top \quad (\text{A.15})$$

$$G_{T_N}(\boldsymbol{\eta}, V) = \left[ \begin{array}{c} \left[ \mathbf{T}_{N_\phi}(\phi, \theta_0, \psi_0, T_0) \Big|_{\phi=\phi_0} \right]^\top \\ \left[ \mathbf{T}_{N_\theta}(\phi_0, \theta, \psi_0, T_0) \Big|_{\theta=\theta_0} \right]^\top \\ \left[ \mathbf{T}_{N_{T_B}}(\phi_0, \theta_0, \psi_0, \mathbf{T}_B) \Big|_{\mathbf{T}_B=\mathbf{T}_{B,0}} \right]^\top \end{array} \right]^\top \quad (\text{A.16})$$

The above control effectiveness matrices can be filled out with Equations A.9 and A.10. Finally, the inversion of Equation A.14 is presented in Equation A.17 and forms the control law.

$$\mathbf{v} = \mathbf{v}_0 + m (G_{L_N}(\boldsymbol{\eta}, V) + G_{T_N}(\boldsymbol{\eta}, \mathbf{T}_B))^{-1} \left( \ddot{\boldsymbol{\xi}}_{\text{ref}} - \ddot{\boldsymbol{\xi}}_0 \right) \quad (\text{A.17})$$